Exhibit 5

Estuaries and Coasts
https://doi.org/10.1007/s12237-019-00634-x

Influences of a River Dam on Delivery and Fate of Sediments and Particulate Nutrients to the Adjacent Estuary: Case Study of Conowingo Dam and Chesapeake Bay

Cindy M. Palinkas[1] · Jeremy M. Testa[2] · Jeffrey C. Cornwell[1] · Ming Li[1] · Lawrence P. Sanford[1]

Received: 23 April 2019 / Revised: 2 August 2019 / Accepted: 11 September 2019

Abstract

Dams impact the magnitude and nature of material transport through rivers to coastal waters, initially trapping much material in upstream reservoirs. As reservoirs fill, trapping decreases and bottom sediments can be scoured by high flows, increasing downstream delivery. This is the case for the Conowingo Dam, which historically has trapped much of the sediment and particulate nutrients carried by the Susquehanna River otherwise bound for Chesapeake Bay but has now reached dynamic equilibrium. While previous studies primarily focus on either delivery of river inputs or their fate in the Bay, this study synthesizes insights from field observations and modeling along the Reservoir-Bay continuum to evaluate potential impacts of infilling on Bay biogeochemistry. Results show most Susquehanna sediment and particulate nutrient loading occurs during high-flow events that occur only ~ 10% of the time. While loading during these events has increased since the late 1970s, consistent with a decreasing scour threshold for Reservoir sediments, loading during low-flow periods has declined. Loads entering the estuary are largely retained within the upper Bay but can be transported farther downstream during events. Reservoir sediments are highly refractory, and inputs of reservoir-like organic matter do not enhance modeled sediment-nutrient release in upper Bay sediments. These findings and an emerging literature highlight the Bay's resilience to large sediment loads during events (e.g., Tropical Storm Lee in 2011), likely aided by ongoing restoration efforts and/or consistently low-moderate recent inflows (2012–2017). Thus, while events can have major short-term impacts, the long-term impact to Bay biogeochemistry is less severe.

Keywords Reservoir · Sediment delivery · River discharge · Biogeochemistry · Storm impacts · Modeling

Introduction

Human influences are pervasive throughout the river-estuary continuum. For example, river channelization, diversions, and levee building alter fluvial morphology and hydrology (Brookes et al. 1983; Gregory 2006; Hudson et al. 2008). Expanded agriculture and/or urbanization can deliver excess sediments and nutrients to estuaries, leading to widespread eutrophication (Barmawidjaja et al. 1995; Kemp et al. 2005; Paerl 2006). Perhaps the greatest human impact on the timing and magnitude of material fluxes from rivers to adjacent receiving basins occurs via dam construction (e.g., Ibàñez et al. 1996; Palinkas and Nittrouer 2006; Vericat and Batalla 2006). Dams initially starve downstream ecosystems of both sediments and particulate nutrients through trapping in upstream reservoirs. Eventually, however, these reservoirs fill (assuming no human intervention), increasing the delivery of sediment and nutrients to downstream ecosystems (Fan and Morris 1992; Yang et al. 2006). Moreover, sediments stored in upstream reservoirs can be scoured during storm events, increasing loads delivered downstream (e.g., Zabawa and Schubel 1974; Palinkas et al. 2014).

The increase in dam construction following World War II has resulted in numerous dams that are rapidly aging and/or filling, prompting much interest in management intervention (e.g., Palmieri et al. 2001). Developing effective management strategies requires holistic consideration of the river-estuary

Communicated by Lijun Hou

Electronic supplementary material The online version of this article (https://doi.org/10.1007/s12237-019-00634-x) contains supplementary material, which is available to authorized users.

✉ Cindy M. Palinkas
cpalinkas@umces.edu

[1] Horn Point Laboratory, University of Maryland Center for Environmental Science, Cambridge, MD, USA

[2] Chesapeake Biological Laboratory, University of Maryland Center for Environmental Science, Solomons, MD, USA

Published online: 05 November 2019

continuum that links upstream actions to downstream ecosystem impacts. For example, large-scale dam removal on the Elwha River dramatically increased fluvial sediment loads and resulted in extensive coastal geomorphological change (Gelfenbaum et al. (2015) and references therein). On the other hand, many questions remain regarding downstream impacts of reservoir infilling.

The upper Chesapeake Bay serves as an excellent natural laboratory within which to address these questions. The Bay and its watershed have experienced many human-induced changes over time, especially since European colonization in the 17–18th centuries (Brush 2009). In particular, land-use changes in the watershed, such as increased deforestation, agriculture, and urbanization, increased sediment and nutrient loads delivered to the Bay. By the mid-1980s, the Bay was receiving 7 times more nitrogen and 16 times more phosphorus than before colonization (Boynton et al. 1995), degrading Bay water quality through eutrophication and decreased water clarity. In response, the Chesapeake Bay Program (CBP) was established in 1983 to identify the sources and extent of pollutants entering the Bay and implement restoration activities to reduce pollutant loads (NRC 2011). More recently, total maximum daily loads (TMDLs) and accompanying watershed implementation plans that include best management practice (BMP) installations have been developed for the Bay and its tributaries (Linker et al. 2013) in an effort to decrease sediment and nutrient loading to the Bay. While quantifying the effectiveness of BMPs can be challenging and depends on specific management goals (Liu et al. 2017), evaluating temporal trends in fluvial loads can lend insight into their performance.

Numerous dams exist along the main tributary to the Bay, the Susquehanna River, including a series of three dams that ends just before the river's confluence with the Bay. The last and largest of these dams, the Conowingo Dam, was constructed in 1928 (Langland and Hainly 1997). While data are scarce for the initial trajectory of filling immediately after construction, plentiful data exist for the infill period for both the Reservoir and upper Bay (Hobbs et al. 1992; Reed and Hoffman 1997; Langland and Cronin 2003; Langland 2009; Russ and Palinkas 2018, among others). Recent work indicates that the Reservoir has reached dynamic equilibrium (net inputs equal net outputs averaged over long time scales) and that particulate loading to the Bay has increased (Hirsch 2012; Zhang et al. 2016). This increased loading is concerning given that the current TMDL requirements, intended to improve Bay water quality, were developed with models that do not include a Reservoir at dynamic equilibrium (Cerco et al. 2013). Increased sediment and nutrient loads from Reservoir infilling could further degrade water quality through eutrophication and reduced bottom oxygen concentrations (Kemp et al. 2005; Kemp et al. 2009; Testa et al. 2014). In addition, large storm events can scour large amounts of sediment from the Reservoir bottom, with potentially deleterious downstream ecosystem impacts (Schubel 1972; Zabawa and Schubel 1974; Orth and Moore 1984).

The timing, magnitude, and mechanisms of material (sediment and its associated nutrients) delivery from the Susquehanna to tidal Chesapeake Bay likely differs between relatively low, "normal" flows and large storms events, especially given human control of the flow at Conowingo Dam, as does its transport and fate in the upper Bay. However, little research has evaluated these differences with a holistic approach that considers the entire river-estuary continuum. This paper is the result of a coordinated, interdisciplinary study that takes this approach and addresses these questions: (1) how has sediment loading to the Bay changed over the last 40 years? (2) are sediments in Reservoir biogeochemically different from those in the upper Bay, and how might they influence Bay biogeochemistry? (3) what controls the transport and fate of Conowingo sediment in the Bay? and (4) what are the likely impacts of watershed and reservoir-derived particulate material on the Bay's biogeochemistry? These questions are evaluated by synthesizing field observations and model results, as well as long-term monitoring data, as shown in Fig. 1. The specific data used to examine each question are (1) river discharge and suspended-constituent (sediment, particulate nitrogen and phosphorus) monitoring data, (2) field observations of sediment biogeochemical characteristics in the Reservoir and upper Bay, (3) transport modeling and field observations of upper Bay sedimentology, and (4) biogeochemical modeling and field observations in the upper Bay. Ultimately, the results of this study can help develop effective management strategies throughout the river-estuary continuum.

Physical Setting

This paper explores the connection of material inputs from the lower Susquehanna River to ecosystem processes in the upper Chesapeake Bay. This connection is highly influenced by a series of three hydroelectric dams that occur along the river from the US Geological Survey (USGS) gauging station at Marietta, Pennsylvania, to its confluence with the Bay (Fig. 2). The reservoirs upstream of the first two dams (Safe Harbor and Holtwood; installed in 1931 and 1910, respectively) filled rapidly after installation and reached dynamic equilibrium (no net change in sediment storage averaged over several years) during ~ 1950 and 1960, respectively (Hainly et al. 1995; Langland and Hainly 1997; Reed and Hoffman 1997; Langland 2009). The last and largest reservoir lies upstream of the Conowingo Dam (installed 1928) and has filled more slowly; however, recent work suggests that it has also reached dynamic equilibrium (Hirsch 2012; Zhang et al. 2013; Zhang et al. 2016).

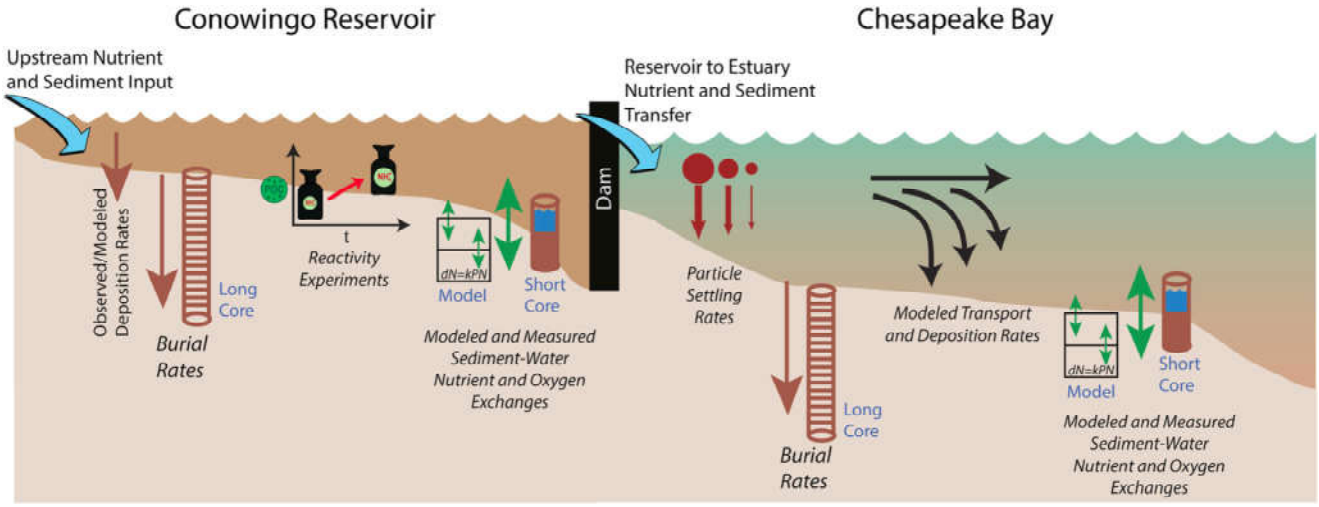

Fig. 1 Conceptual model of the various methods used in this study and their relationships to components of the Conowingo Reservoir-Chesapeake Bay continuum. See "Methods" for details of individual methods

Infilling of Conowingo Reservoir was most rapid in the upper portion after installation (Langland 2009) but is now focused largely in the lower portion (Palinkas and Russ 2019). As a result, surficial bottom sediments generally grade from sands in the upper portion to muds in the lower portion. Sediment deposition within the reservoir is inherently linked to delivery from the Susquehanna River, which is highest during the spring freshet and minimal during summer, punctuated by extreme flood events (Hirsch 2012; Cheng et al. 2013; Zhang and Blomquist 2018) that can scour significant amounts of bottom sediment from the reservoir. Significant scour occurs when river discharge exceeds ~ 11,300 m^3/s (400,000 cfs; Hainly et al. 1995), but this threshold has likely lowered over time and fine sediments are mobilized at lower flows (Hirsch 2012). Floods of this size generally occur every ~ 5 years, with notable past occurrences in 1972 (Tropical Storm (TS) Agnes), 1996 (winter ice jam), 2004 (Hurricane Ivan), and 2011 (TS Lee). The highest recorded Susquehanna River discharge was associated with TS Agnes, exceeding 28,317 m^3/s (1,000,000 cfs) and scouring 13.5×10^6 t of bottom sediment (Langland 2015). The second highest discharge was associated with TS Lee, exceeding 16,990 m^3/s (600,000 cfs) and scouring 4×10^6 t of bottom sediment (Cheng et al. 2013; Palinkas et al. 2014). The resulting sediment load delivered to the Bay, composed of both watershed and scoured Reservoir sediments, resulted in a sediment plume that appeared to extend at least halfway down the Bay in satellite images. The fate of TS Lee sediments in the Bay was investigated through both field (Palinkas et al. 2014) and modeling (Cheng et al. 2013) approaches, finding that most sediment was retained in the upper Bay, but fine sediment was more widely dispersed, resulting in a thin drape of sediment on the bottom extending to mid-Bay. The second largest storm during the past 15 years was Hurricane Ivan (2004), which had peak discharge of ~ 15,000 m^3/s. Ivan produced heavy precipitation over the Chesapeake Bay watershed, with maximum accumulation of 25 cm. A satellite image showed a sediment plume spreading over the upper and mid parts of Chesapeake Bay, but the resulting sediment deposit was not sampled.

Conowingo Dam is run as a peak-production hydroelectric plant, with daily high/low river discharges through the outlet. This variability is integrated on longer time scales, such that discharge patterns are similar to those at Marietta. During high flows, the first flood gate is typically opened at ~ 2446.5 m^3/s (86,400 cfs; Velleux and Hallden 2017), which is the discharge used to define "events" in this paper. Several recent modeling studies have focused on trends in sediment and nutrient delivery over the Dam, especially with regard to trapping in the Reservoir. Conowingo Reservoir historically trapped much of the sediment and nutrient load to the Chesapeake. However, recent studies indicate that discharge of these materials from Conowingo has remained relatively steady or perhaps even increased, despite declines at the reservoir inlet from watershed reductions (Hirsch 2012; Zhang et al. 2016). This implies reduced trapping within the reservoir, consistent with results from repeat reservoir bathymetric surveys (Langland 2015).

In the uppermost Bay, Susquehanna discharge has formed a subaqueous delta, referred to as the Susquehanna Flats, a shallow, sandy region colonized by submersed aquatic vegetation (SAV). SAV beds on the Flats were historically dense but disappeared after TS Agnes (Bayley et al. 1978). They made a resurgence in the early 2000s, due to improved water quality from a combination of resource management actions and several dry years (Gurbisz and Kemp 2014), and have been present ever since, even during extreme events (TS Lee; Gurbisz et al. 2016). These beds modulate sediment input from the Susquehanna River to the upper Bay, trapping sediment during the growing season (typically ~April–October) but

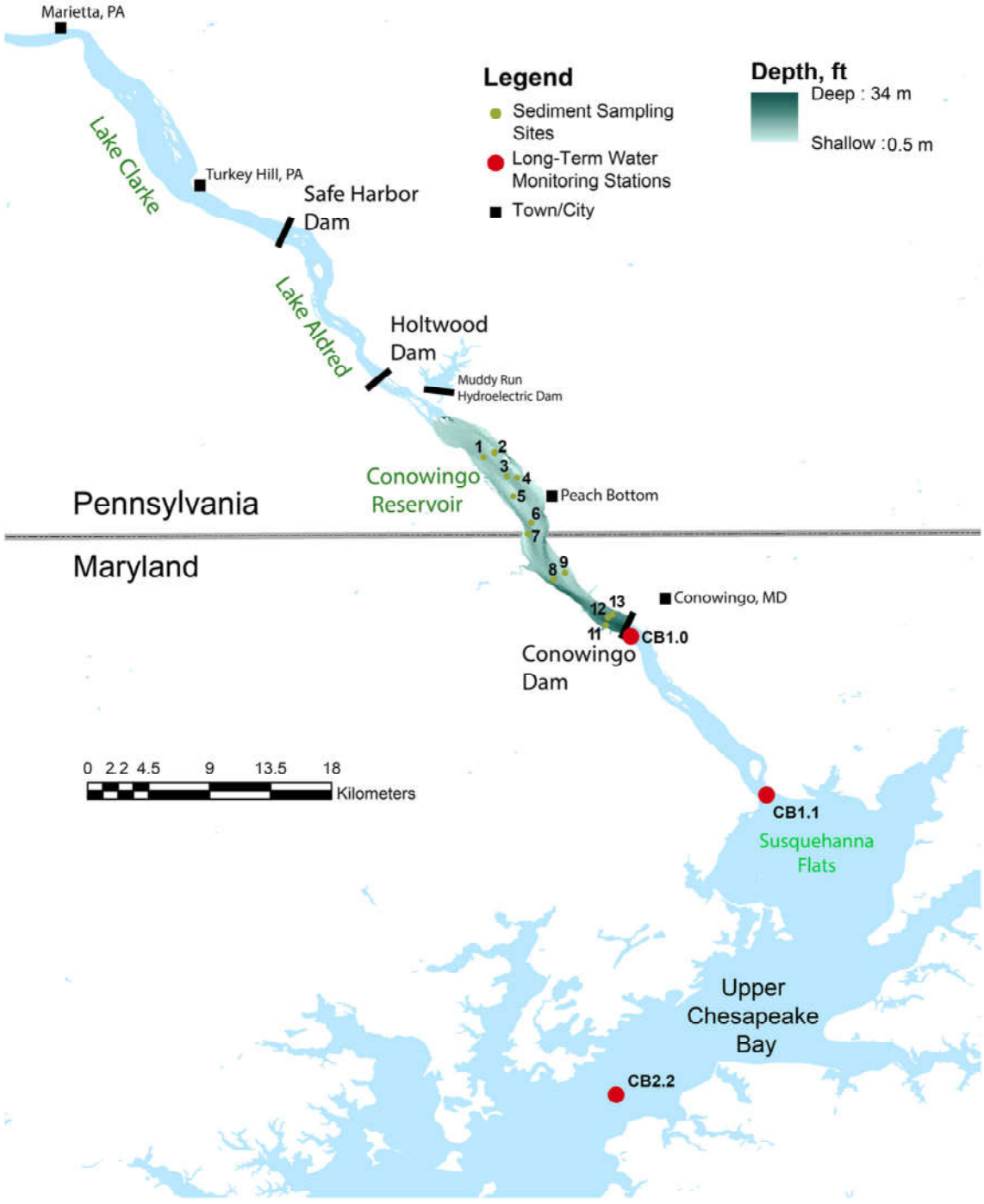

Fig. 2 Site locations in the lower Susquehanna River and upper Chesapeake Bay. Locations of hydroelectric dams on the Susquehanna River are given by black bars. Brown circles show locations of sediment sampling sites in Conowingo Reservoir (geochronology and sediment character reported in this study and in Palinkas and Russ (2019), sediment-water fluxes in this study). Red circles indicate locations of long-term water quality monitoring data used in this study

allowing sediment bypass over winter (Russ and Palinkas 2018).

Sedimentation rates in the upper Bay have varied throughout time, responding to changes in land use and storms. Rates increased dramatically after European colonization and related land clearance, but they decreased after 1930 due to farm abandonment and soil conservation (Brush 1989; Brush 2001), as well as construction of Conowingo Dam. The signatures of large storms and hurricanes are preserved in sediment cores, especially after TS Agnes and Lee. The thickest

deposits are located upstream of the estuarine turbidity maximum (ETM), with maximum thickness of 20–30 cm after TS Agnes (Zabawa and Schubel 1974) and 4–5 cm after TS Lee (Palinkas et al. 2014).

The ETM is the dominant driver of sediment transport dynamics in upper Chesapeake Bay. First reported in the late 1960s (e.g., Schubel 1968), upper Bay ETM dynamics have been studied (Elliott 1978; Sanford et al. 2001; Cronin et al. 2003; North et al. 2004) and modeled (Park et al. 2008; Cerco et al. 2013) by numerous researchers since then. ETMs are very efficient traps for suspended particles carried into estuaries with the river flow. The upper Bay ETM results from convergent near-bottom transport of settling particles due to asymmetrical tidal resuspension near the limit of salt (Sanford et al. 2001). The efficiency of ETM trapping increases as particle settling speeds increase due to flocculation and agglomeration of fine riverine particles, caused by increases in both electrochemical and biogeochemical stickiness as fresh river waters encounter and mix into salt water (Schubel and Kana 1972; Sanford et al. 2005; Malpezzi et al. 2013). ETMs are dynamic features, rapidly migrating downstream due to pulses of river flow and down-estuary winds while rebounding almost as quickly as the downstream forcing dissipates, albeit with a scale-dependent lag (Nichols 1977; Elliott 1978; North et al. 2004). The upper Bay ETM is a very efficient sediment trap in the long term, likely due to the large scale of the system. Particles deposited over the shallow shoals adjacent to the channel are easily resuspended due to wind-wave forcing (Sanford 1994), likely focusing back into the deep shipping channel. Particles that escape downstream in moderately large events tend to be transported back upstream by the combination of tidal and estuarine circulations (Nichols 1977). Maintenance dredging of the upper Bay shipping channel likely removes a large fraction of the accumulating sediment (Sanford et al. 2001). The net result may approach near complete riverine sediment trapping (Donoghue et al. 1989), with some unknown but small fraction lost to the mid-Bay during extreme freshwater flow events.

The eutrophication of Chesapeake Bay has been well documented (Hagy et al. 2004; Kemp et al. 2005) and is associated with elevated nutrient inputs from its large watershed (166,530 km^2) that spans several states in the mid-Atlantic region of the USA. Increased degradation of the Bay was documented in the 1970s and 1980s, following the identification of large-scale declines in submersed aquatic vegetation (SAV) (Kemp et al. 1983) and mapping of extensive low-oxygen areas in the mainstem of the estuary (Officer et al. 1984). While declines in commercial finfish and wild bivalve extraction were early identified as features of the Bay's decline, elevated inputs of dissolved nitrogen and phosphorus from the watershed beginning in the late 1960s and early 1970s were identified as causative agents for many of the lost habitats in the estuary. Following more than three decades of extensive monitoring of dissolved oxygen, nutrient concentrations, SAV coverage, and watershed inputs, it has become apparent that several features of the Bay's ecosystem have began to transition toward a less-eutrophic state (Orth et al. 2017; Testa et al. 2018; Zhang et al. 2018).

Methods

This paper synthesizes field observations, model results, and long-term monitoring data as conceptualized in Fig. 1. Details of specific methods are presented below.

Inputs to Estuary

River Discharge and Suspended Sediment Concentrations (SSC)

Susquehanna River discharge has been measured at the Conowingo Dam outlet by the USGS (http://waterdata.usgs.gov; station 01578310) since October 1967. Corresponding suspended sediment concentrations (SSC) have been measured since 1978, with variable frequency throughout the years. Generally, data were available for at least 1 day per month and more frequently during high-flow events; however, there are some gaps in the records.

For consistency, this study considered discharge and SSC data only between 1 Jan 1978 and 31 December 2017. Rating curves (SSC versus corresponding river discharge) were developed for 5-year intervals (i.e., 1968–1972, 1973–1977, etc.), following the approach of Warrick (2015). Because relatively few SSC measurements are available for each year, 5-year intervals were chosen as a compromise between temporal resolution and robustness of the data set. The main difference between the Warrick (2015) approach and more traditional approaches (e.g., Syvitski and Morehead 1999) is the use of discharge-normalized data (Q_{GM}) in the regression between log-transformed river discharge (Q) and SSC (C):

$$C = \ddot{A}(Q/Q_{GM})^{b}, \quad (1)$$

where $\hat{a}$ is the vertical offset parameter and has units of mg/L, equivalent to the SSC of the middle of the sample distribution, b is the unitless rating parameter found from regression (Syvitski and Morehead 1999), and Q_{GM} is the geometric mean of all Q values in the entire record (uniform for all time intervals). These curves were calculated for three cases: (1) all flows, (2) "normal" or non-event flows, and (3) high flows during flood events. A discharge of 2446.5 m^3/s was used to separate normal (< 2446.5 m^3/s) and event (> 2446.5 m^3/s) flows, corresponding with opening of the first crest gate (Velleux and Hallden 2017) and the 90th percentile of flows past Conowingo from 1968 to 2017. These rating curves were

used to calculate daily SSC values from river discharge measurements. Daily sediment loads (product of SSC and river discharge) were then calculated and summed over individual years and 5-year periods.

Particulate Phosphorus (PP) and Nitrogen (PN)

Particulate phosphorus (PP) and nitrogen (PN) data were obtained from data associated with Zhang et al. (2015) and archived by Zhang and Ball (2014). This archive contains raw particulate phosphorus and nitrogen concentrations from the USGS River Input Monitoring Program (USGS 2013). Like SSC, these concentrations were not continuously measured and were assumed to represent average daily conditions. Comparison of these concentrations with their corresponding river discharge showed wide variability, precluding establishment of statistically robust relationships from which daily loads could be calculated. Instead, daily loads of both PP and PN were obtained from the WRTDS model (Zhang et al. 2015), which accounts for variability in these parameters with both time and discharge. These data were available only prior to April 2013, excluding the 2013–2017 time period from further consideration.

Particle Settling Velocities

All other things being equal, particle settling velocity is the most important factor determining the transport distance of suspended particles (Mcnair and Newbold 2001). Prior to this study, however, particle settling velocities had never been directly measured at the Conowingo Dam. Samples were collected for particle settling velocity experiments during three moderately high flow events in 2015 and 2016, over a total of seven sampling days. On each sampling day, suspended particles were collected at the turbine outlets on the downstream side of Conowingo Dam, where historical USGS samples were collected, and from a stilling well located on the upstream side of the dam between two spill gates. At both locations, 5-L sample bottles were filled for settling experiments; additional samples were collected at the downstream site for standard disaggregated particle size analysis by the USGS (Poppe et al. 2005).

Settling velocity experiments usually occurred within an hour of collection; samples were refrigerated in the event of any short delay. These experiments were carried out on-site using a settling tube apparatus based on the classic Owen tube (Owen 1976), modified for field work in upper Chesapeake Bay (Malpezzi et al. 2013), and then modified again for this study. The settling tube apparatus consisted of a pair of 5-L Niskin bottles attached vertically to an aluminum frame. The bottom stoppers were machined to a funnel shape internally, with a sampling port attached at the lower end of the funnel. The top stoppers were attached flexibly to allow water and suspended sediment samples to be introduced quickly and cleanly. A jacket of reflective bubble wrap around each tube minimized the development of internal circulations due to contrasts between inside and outside temperatures.

At the beginning of each experiment, water samples were shaken gently to resuspend any settled particles and poured into the settling tubes, completely emptying the sample bottles to avoid missing any rapidly settling particles. A timer was started for each tube, with staggered starts to allow sampling at matched intervals after time 0. Ten water samples were withdrawn from the bottom port of each tube into prewashed 0.5-L sample bottles at nine geometrically spaced time intervals (two bottles at the last time interval). Analysis procedures used for bottom withdrawal settling tube experiments were first described by Owen (1976). A spreadsheet implementation of these techniques was used (Malpezzi et al. 2013), as well as a Matlab© curve-fitting implementation (Malarkey et al. 2013). Both techniques yielded similar estimates of the settling distribution of suspended-sediment mass (Fig. S1). Based on these results, all settling experiment results were divided into four categories of settling speeds: < 0.01 mm/s (the last sample bottle), 0.01–0.2 mm/s, 0.2–2 mm/s, and > 2 mm/s; mass fractions were calculated for each category for all experiments.

Settling velocities were also estimated for the samples collected simultaneously and analyzed by USGS for disaggregated particle size distributions. We used Stokes settling velocity equation for clays and silts and the approximate large particle expression of Soulsby (1997) for sand-size particles. These data were then divided into the same four settling velocity categories as above for direct comparison with the settling experiment data. Equivalent particle size categories were calculated for each of the four settling velocity categories using these same expressions, resulting in equivalent particle size bins of < 0.004 mm, 0.004–0.016 mm, 0.016–0.052 mm, and > 0.052 mm, respectively.

We also obtained data from 32 samples collected by USGS on 19 dates between 1979 and 2015 for which disaggregated particle size data were available, along with corresponding river discharge and SSC data. The USGS data were stored as cumulative percent distributions (total percent finer than each of ten sizes). We calculated the percent of suspended sediment mass between successive sizes by difference. We then binned the mass fractions into the four size intervals defined above and calculated a characteristic mass-weighted settling speed for each size range.

Fate of Sediment in the Estuary

Sedimentology

Four box cores were collected in August 2015 in the upper Bay; gravity cores were collected at these sites and three

additional sites in April 2016 (Fig. 3). Both 2015 and 2016 reflected conditions during "normal" years (i.e., no major flood events); core locations were co-located with those in Palinkas et al. (2014) to discern differences between normal and flood conditions. All cores were sectioned immediately after recovery and transported to the lab for further analyses. All cores were analyzed for grain size and ^{7}Be (half-life 53.3 days); gravity cores were also analyzed for ^{210}Pb (half-life 22.3 years). Grain-size measurements were made by wet-sieving samples at 63 μm to separate the mud (silts and clays; < 63 μm) and sand (> 63 μm) components. The mud fraction was then analyzed with a Sedigraph III (Coakley and Syvitski 1991), and the sand fraction was dry sieved from 64 to 500 μm via a standard set of 13 sieves. All data were combined to calculate the median diameter of sediment. Event- and seasonal-scale sedimentation was examined with ^{7}Be, which is produced by cosmic rays in the atmosphere and attaches to terrestrial sediments during wet (rainfall) and dry deposition (Olsen et al. 1986). Because nearly all of the ^{7}Be is associated with particulates (Kaste et al. 2002), the presence of ^{7}Be in aquatic sediments indicates that they had been on land within ~ 250 days (4–5 half-lives, assumed limit of detectability). ^{7}Be activities were measured via gamma spectroscopy of the 477.7 keV photopeak, using a calibrated Canberra germanium detector and following the procedure of Palinkas et al. (2014). Depth-integrated activities were used to calculate sediment deposition rates as in Palinkas et al. (2005). Decadal-scale sediment accumulation rates were determined with ^{210}Pb (half-life 22.3 years), measured via alpha spectroscopy, assuming a constant supply of unsupported ^{210}Pb to the

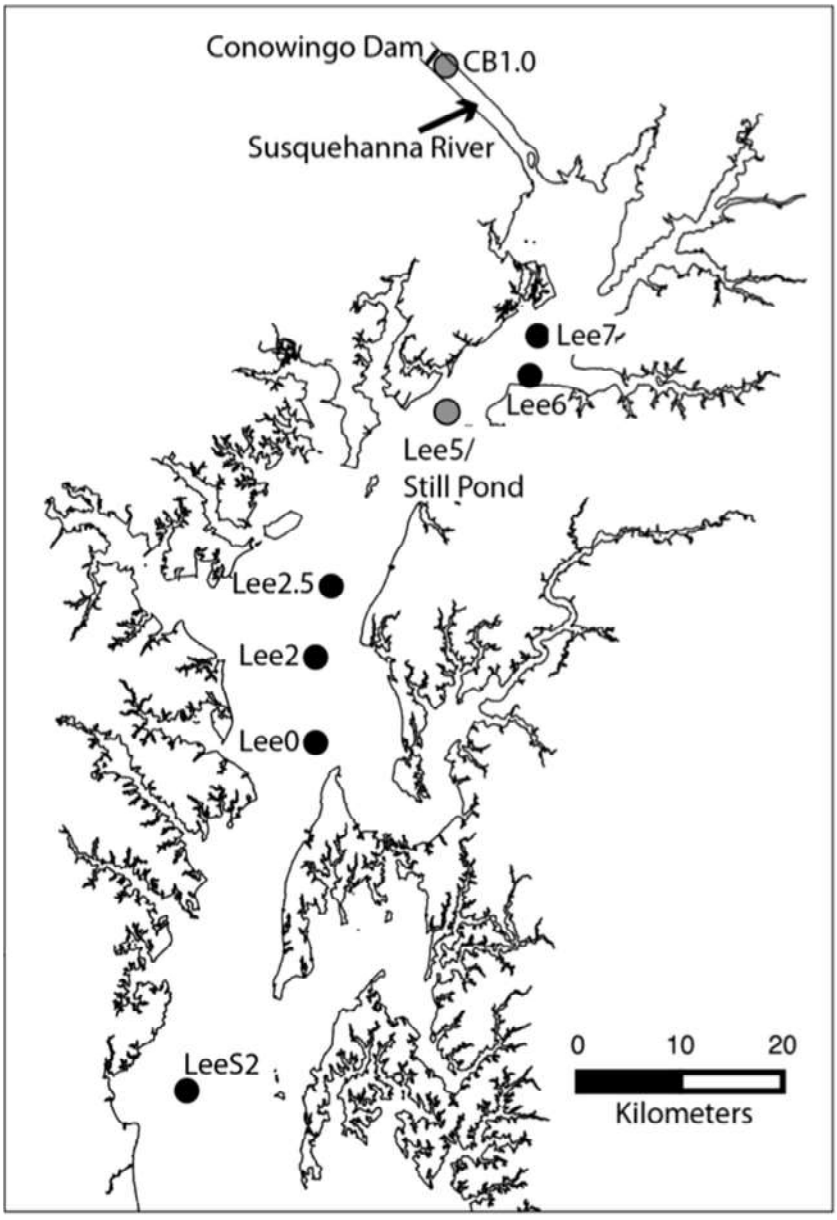

Fig. 3 Locations of sediment cores (black circles; labeled as Leex) and monitoring stations (gray circles) used in this study. Note that core Lee5 and the monitoring station at Still Pond are co-located. Box cores were collected at Lee7, Lee5, Lee2.5, and LeeS2; gravity cores were collected at all core locations

sediment and steady-state sedimentation (Appleby and Oldfield 1978). Accumulation rates were reported in Russ (2019) and Russ and Palinkas (2018).

Transport Modeling

The Coupled Ocean-Atmosphere-Wave-Sediment Transport (COAWST) modeling system (Warner et al. 2008; Warner et al. 2010) was used to configure a model for Chesapeake Bay and its adjacent shelf. COAWST consists of a mesoscale atmosphere model, a regional ocean model, a model for simulating surface waves, a sediment transport model, and a dynamic coupler to exchange data fields between the submodels. It has been used in a number of studies on sediment dynamics in coastal oceans, during both storm and non-storm conditions (e.g., Harris et al. 2008; Ganju et al. 2009; Olabarrieta et al. 2011; Cheng et al. 2013; Sclavo et al. 2013; Feddersen et al. 2016).

In this implementation of COAWST (Xie et al. 2018), observed wind speeds at buoys and weather stations throughout Chesapeake Bay and its surrounding land were used instead of the hindcasts from a regional atmosphere model, and the regional ocean model was based on Regional Ocean Modeling System (ROMS) (Haidvogel et al. 2000; Shchepetkin and McWilliams 2005; Shchepetkin and McWilliams 2009). The ROMS model for Chesapeake Bay has been validated against observational data (e.g., Li et al. 2005; Li et al. 2006; Zhong and Li 2006). In this study, we used a finer-resolution version of this model (Cheng et al. 2013; Xie et al. 2018), with 240 × 160 horizontal grids and 20 vertical layers. The model was forced by freshwater inflows at river heads, tidal and non-tidal flows at the offshore boundary, and winds and heat exchanges across the water surface. At the upstream boundary of the eight major tributaries, freshwater inflows at USGS gauging stations were prescribed. The wave model was Simulating WAves Nearshore (SWAN) (Booij et al. 1999), which simulates wind-wave generation and propagation in coastal waters, including the processes of refraction, diffraction, shoaling, wave–wave interactions, and dissipation. SWAN was configured to have the identical horizontal grids as ROMS. The SWAN model was forced by historical Wave Watch 3 data (archived at ftp://polar.ncep.noaa.gov/pub/history/waves/incident) at the offshore boundary and by the observed winds at the sea surface. The sediment modeling component was the Community Sediment Transport Modeling System (CSTM) (Warner et al. 2008), which includes algorithms for suspended sediment and bedload transport due to current and wave–current forcing, enhanced bottom stress due to surface waves, and a multiple bed model to track stratigraphy and morphology. Sediments can be introduced into the model domain through rivers and erosion from seabed. For fluvial sediment, we considered only the Susquehanna River, which is the only river discharging sediment directly into the main stem of the Bay (sediments from other tributaries are largely entrapped within them; Biggs 1970; Schubel and Carter 1977). Fluvial sediments were divided into three classes (clay, fine silt, and coarse silt), each represented by a grain size and settling speed corresponding to the settling velocity analyses described above. Because our study focused on fluvial sediment, the seabed is simplified and initialized with uniformly distributed silt with a single grain size of 0.022 mm (North et al. 2004). Resuspension of bottom sediment acted as the background for the suspended sediment in the Bay. For high SSC, the effect of suspended sediment to water density was included by treating the water as a water-sediment mixture. Relevant parameters of the sediment module are listed in Table 1.

Sediment Biogeochemistry and Exchange with Water Column

Sediment-Water Fluxes in the Reservoir and Estuary

The sediment exchange of oxygen, nitrogen, and phosphorus was determined in the Conowingo Reservoir on five dates (May, July, September 2015; April 2016), in Lakes Clarke and Aldred in April 2016 and in the upper Bay in August 2015 and April 2016. Reservoir cores were collected at 6–13 sites using a Soutar-style plastic box corer in fine-grained deposits and a pole corer in shallow coarse-grained deposits (Cornwell et al. 2014). Bay cores were collected with a HAPS corer (KC Denmark), sub-coring the stainless steel tube (13.6 cm diameter) for smaller flux cores. Sediments were collected for incubation in 6.3-cm diameter, 30-cm tall acrylic flux cores that were filled with ~ 15 cm of sediment. At each reservoir station, surface- and deep-water measurements of conductivity/salinity, temperature, and dissolved oxygen were made using a YSI multiparameter sonde. Water was collected via pump from two reservoir locations for use in sediment incubations and from multiple locations in the Bay. After collection, cores were placed upright in large insulated containers full of site water until placement in a temperature-controlled room later that day. Core-incubation procedures are described in detail elsewhere (Owens and Cornwell 2016) and briefly described here. Cores were submersed in site water and bubbled overnight in the dark at field temperatures. At the beginning of the incubation phase, stirring lids were attached to the cores and a time course of overlying water chemistry was determined initially under dark conditions for 4–6 h. Additional site-water-only "blank" incubations were set up from each aerobic coring site to correct for biogeochemical processes occurring in the water. Water analyses included gas ratios (O_2/Ar, N_2/Ar) via MIMS (membrane inlet mass spectrometry; Kana et al. 1994) and nutrients (nitrate plus nitrite (NO_x^-), ammonium (NH_4^+), and soluble reactive phosphorus (SRP)) using conventional colorimetric methods

Table 1 Parameters for the sediment-transport model. Particle settling velocities and grain sizes are representative of the classes observed in the settling velocity experiments. The flow-dependent fractions f_1-f_4 are described in the results and shown in Fig. 5

Fluvial sediment				Bay bottom sediment
Sediment parameters	Clay	Fine silt	Coarse silt	
Grain size (mm)	0.002	0.007	0.0265	0.022
Settling velocity (mm/s)	0.003	0.045	0.632	0.31
Critical shear stress (N/m^2)	0.013	0.022	0.09	0.49
Erosion constant ($kg/m^2/s$)	4×10^{-5}	4×10^{-5}	4×10^{-5}	5×10^{-5}
Fraction (%)	f_1	f_2	$f_3 + f_4$	100
Bottom porosity	0.91	0.91	0.91	0.91

(Parsons et al. 1984; García-Robledo et al. 2014). Gas and nutrient flux rates were calculated from core area and volume, and the slope of solute/gas versus time.

Characterization of Sediment Composition and Reactivity

The reactivity of particulates with respect to the potential bioavailability of phosphorus (P) and nitrogen (N) was assessed by chemical characterization (P) and time courses of anaerobic ammonium production. Sulfate concentrations from increasing salinity enhance the sulfate respiratory pathway and the resultant hydrogen sulfide converts Fe oxides into iron-sulfide minerals (Cornwell and Sampou 1995). Iron-sulfide minerals adsorb soluble reactive P poorly relative to Fe oxides, and as a result, P is often released to solution (Roden and Edmonds 1997) and to overlying water (Lehtoranta et al. 2009). A sulfide-reactive pool was determined by the addition of hydrogen sulfide (Vulgaropulos 2017). Both sediments and suspended particulates were characterized for rates of anaerobic NH_4^+ production using sediment slurries and particulates filtered from the water column, with a time course used to determine rates (e.g., Burdige 1991).

Biogeochemical Modeling

A sediment biogeochemical model (SFM) was used to evaluate rates and controls on nutrient storage, biogeochemical transformation, and release for reservoir and upper Bay sediments. SFM is a two-layer representation of sediment biogeochemical processes that simulates carbon, nitrogen, phosphorus, oxygen, silica, and sulfur dynamics. SFM has been successfully utilized in diverse Bay environments under different conditions (e.g., temperature, salinity, oxygen, and depth) to understand sediment responses to particulate-matter deposition (Brady et al. 2013; Testa et al. 2013). SFM numerically integrates mass-balance equations for chemical constituents in two functional layers: an aerobic layer near the sediment-water interface of variable depth (H_1) and an underlying anaerobic layer that is equal to the total sediment depth (10 cm) minus the depth of H_1. Details of the model and its implementation can be found in other recent publications (Brady et al. 2013; Testa et al. 2013; Testa et al. 2014).

SFM simulations were executed at 13 stations in the reservoir and one station in the upper Bay (Still Pond; Fig. 3) where sediment-water flux experiments were conducted (see above; Testa et al. 2013). Model simulations were run for the 1985–2015 period using the following schemes to estimate boundary conditions. For the overlying water, we generated a climatology of water-column nutrient and oxygen concentration measurements from 1985 to 2015 at the Conowingo Dam outlet (CB1.0; Fig. 3). Concentrations at CB1.0 were assumed to be representative for the reservoir; where possible, concentrations from CB1.0 were compared to those from the 2015 field campaigns with good agreement (Testa and Kemp 2017). To estimate the depositional fluxes of bulk pools of organic carbon, nitrogen, and phosphorus, we tested three different schemes for estimating matter deposition rates. In the first scheme, we assumed a constant deposition rate to Conowingo and Upper Bay sediments based upon previous estimates made for the Upper Chesapeake Bay (Brady et al. 2013). In the second scheme, we generated a seasonal cycle of deposition that followed the local, historically observed chlorophyll-a pattern in time but whose magnitude was similar to direct sediment trap estimates made previously in the Conowingo Reservoir or previous model simulations (Fig. S2; Brady et al. 2013; Boynton et al. 1984; Testa and Kemp 2017). We repeated this annual cycle for each year in the simulation period. In the third scheme for the Reservoir only, we used estimates of TN input to the reservoir made at Marietta, Pennsylvania (upstream of the 3 reservoir system), assumed a constant fraction of the load was particulate in nature, assumed a fixed C/N/P ratio based on prior reservoir measurements (Boynton et al. 1984), and divided these inputs by the area of the reservoirs. In this scheme, we assumed that deposition occurred uniformly in the Reservoir and we averaged the input data over a 90-day period to yield constant 3-month periods of deposition (Fig. S3). In effect, we used the time-series of inputs derived at Marietta to provide the temporal variability and scaled the overall input to values constrained by simulations using the first two schemes.

We estimated organic-matter reactivity in the depositing material by simultaneously re-estimating the magnitude of organic matter deposition and the relative fraction of the three reactivity pools within the deposits. 'G1' indicates labile organic material that reacts at the timescale of 30 days, 'G2' is refractory material that decays on the time scale of 18 months, and 'G3' is very low reactivity organic matter that decays at very long timescales. Model simulations in each suite of the simulations were analyzed to maximize agreement between observed and modeled sediment-water nutrient and oxygen fluxes and sediment organic matter nutrient and carbon fractions. We obtained estimates of bottom sediment carbon, nitrogen, and phosphorus content from Edwards (2006) and estimates of carbon, nitrogen, and phosphorus content of water-column particles from Boynton et al. (1984). We did not use the sediment percent carbon data, given the observed presence of coal in many sediment cores (Edwards 2006).

Results

Inputs to the Estuary

River Discharge and Suspended Sediment Concentrations (SSC)

Mean daily Susquehanna River discharge (flow on a given day averaged over the entire record) from 1978 to 2017 was highest during the spring freshet (~ 2000–2600 m^3/s), lowest during the summer and early fall (< 500 m^3/s), and intermediate in winter (~ 1000–1500 m^3/s); however, discharge on individual days varied over several orders of magnitude, from a minimum of 20.3 m^3/s on 2 Nov 1980 to a maximum of 20,064.7 m^3/s on 9 Sept 2011. Concurrent SSC measurements were made on 998 days out of the 14,610 days from 1978 to 2017. Sampling frequency of these measurements varied over the years but was biased toward higher discharges, such that the annual average discharge for days with SSC measurements was twice as high as that which includes the entire record. Even so, linear temporal trends were similar between the two data sets (see Table S1 for statistical results), whether discharge was averaged over 1- or 5-year periods. Specifically, average river discharge during events decreased over time, increased for non-events, and had no significant trend for all flows together.

SSC ranged from a minimum of 1 mg/L, which may have reflected the lower measurement limit and occurred on 5 days (12 Feb 1980, 15 Jan 1986, 2 Feb 2000, 10 Dec 2012, and 4 Feb 2003), to 3680 mg/L on 20 August 2004. While there were no consistent temporal trends in annual-average SSC for all flows or event flows, years with large scour events were notable outliers, particularly 2004 (annual average SSC 235 ± 888 mg/L) and 2011 (annual average SSC 245 ± 601 mg/L). These extremes were not as apparent in the 5-year averages, which significantly increased for event flows after 1982 (first interval; note SSC data were unavailable for events in 1978 or 1982). To minimize the potential confounding effect of scour, separate regression models were built for event flows below the nominal scour threshold of 11,300 m^3/s (400,000 cfs), with no trends in annual-average SSC but a significant increase in the 5-year average after 1982 ($p = 0.06$, $R^2 = 0.53$). Trends for flows above the scour threshold were not evaluated, since there were only 13 SSC observations during these conditions. Both the 1- and 5-year averaged SSC decreased significantly for non-event flows.

The relationship of SSC to river discharge was first evaluated simply by calculating their ratio, focusing on changes over time rather than the absolute values, which minimizes the influence of climatic variability (i.e., higher particulate loads during wet years) (Fig. 4; Table S1). Both 1- and 5-year average ratios significantly decreased for all flows and non-event flows but had no trend for event flows. Years with large scour events (e.g., 2004, 2011) were notable outliers; annual-average ratios for event flows below the scour threshold did not have a significant relationship with time, but 5-year average ratios showed a significant increase after 1982. Alternatively, changing relationships of SSC and river discharge were assessed through a rating-curve analysis (Eq. 1). For this analysis, individual curves were calculated for each 5-year time period for event and non-event flows; changes in the rating parameters $\hat{a}$ (vertical offset) and b (slope) of these models were then evaluated. For all flows, values of $\hat{a}$ significantly decreased over time ($p = 0.02$, $R^2 = 0.61$), indicating that recent SSC values are lower than in the past for a given flow, but the value of b had no trend. This was also true for non-event flows—significant decrease in $\hat{a}$ ($p = 0.001$, $R^2 = 0.84$) but no trend for b. Neither $\hat{a}$ nor b had a significant temporal trend for events.

Gaps in the SSC measurement record were filled using the corresponding rating curve for the year and flow conditions; daily sediment loads were calculated by the product of SSC and river discharge, then summed for each 1- and 5-year interval. Total annual sediment loads (all flows) varied from 0.22×10^6 t (2001) to 11.5×10^6 t (2011). For individual years, event flows contributed between 12% (2009) and 98% (2011) of the total load, with an average contribution of 62.0 ± 23.7%. Five-year total sediment loads (all flows) varied from 2.1×10^6 t (2013–2017) to 14.5×10^6 t (2008–2012), with an average event contribution of 72.3 ± 17.5%. For comparison, event flows occurred on roughly 10% of the days from 1978 to 2017 (1338 days out of 14,610 total days in the record).

Particulate Phosphorus (PP) and Nitrogen (PN)

Observed daily PP concentrations varied from 0.002 mg/L (2 Sep 1992) to 2.3 mg/L (8 Sep 2011), with highest values occurring during large scour events. Annual average PP varied

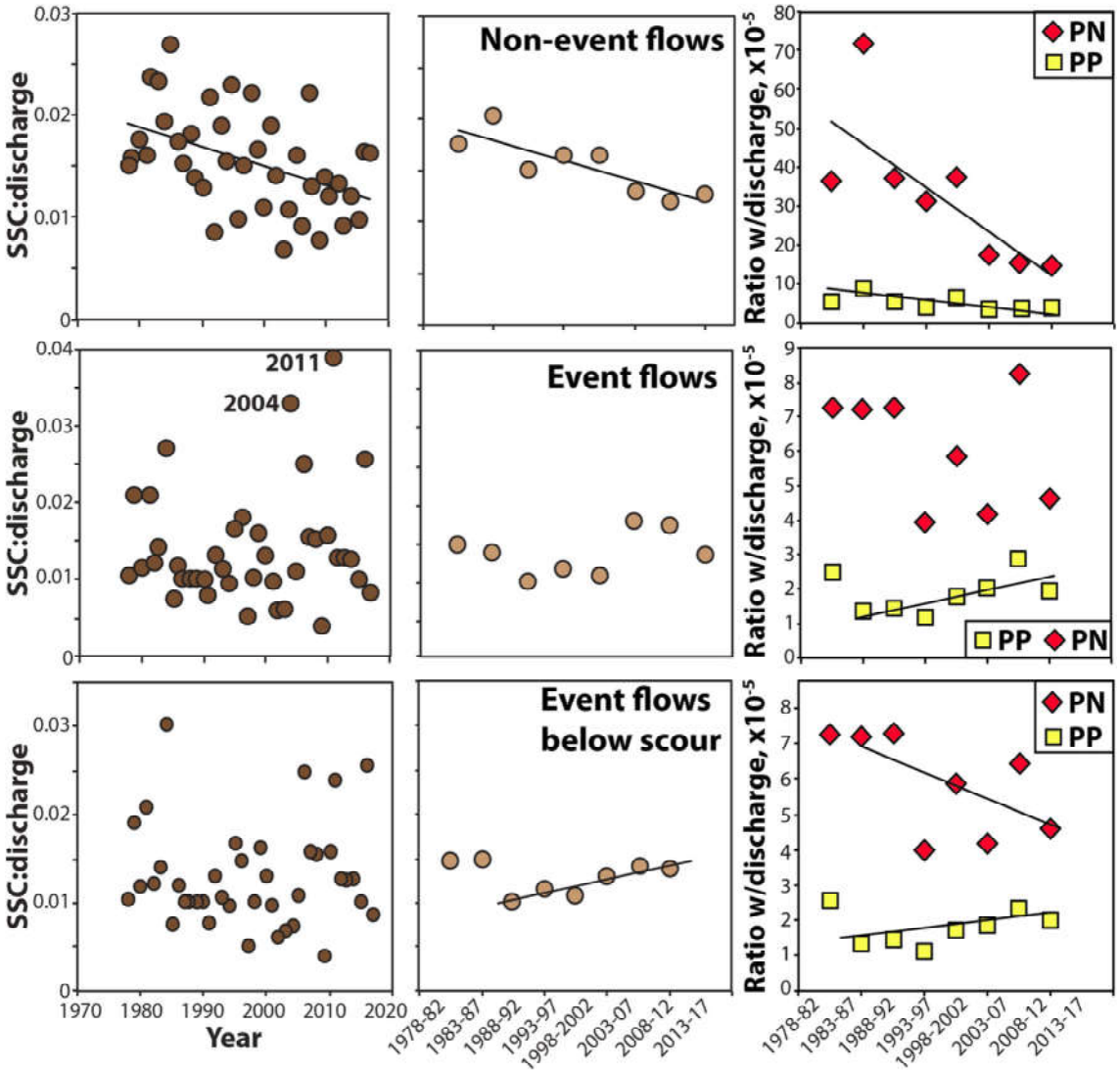

Fig. 4 Ratios of suspended sediment concentration (SSC) and nutrient concentrations to river discharge for (top to bottom): non-event flows, event flows, event flows below the scour threshold. For each row, the left hand panel shows annual averages of SSC ratios, the middle panel shows 5-year average SSC ratios, and the right hand panel shows 5-year averages of particulate nitrogen (PN; red diamonds) and particulate phosphorus (PP; yellow squares) concentrations. Significant linear regression fits are shown; see Table S1 for associated statistical parameters

from 0.02 ± 0.02 mg/L (1997) to 0.22 ± 0.46 mg/L (2011), with notably high values in 2004 (0.12 ± 0.3 mg/L) and 1981 (0.13 ± 0.11 mg/L). Correspondingly, 5-year average PP was highest in 1978–1982 (0.08 ± 0.09 mg/L) and 2008–2012 (0.09 ± 0.03 mg/L). However, the highest annual-average ratio of PP concentrations to river discharge occurred in 1998, which did not include a scour event, and the lowest annual-average ratio was in 1996, which did include a scour event. Annual-average ratios decreased for all flows and non-event flows (Table S1). For event flows, these ratios decreased significantly for the first ~ 10 years (1979–1987; $p = 0.04$, $R^2 = 0.53$; note that PP observations were not made during events in 1978 or 1982), then increased significantly for the rest of the record (1988–2017; $p < 0.001$, $R^2 = 0.34$). Ratios averaged over 5 years showed no consistent temporal trends for all flows but significantly decreased for non-event flows. For event flows, 5-year average ratios significantly increased ($p = 0.06$, $R^2 = 0.55$) but only after 1982, which had a relatively high ratio.

Observed PP concentrations varied widely with river discharge, regardless of flow condition, limiting confidence in regression models. Instead, daily values were obtained from the WRTDS model (Zhang et al. 2015), which accounts for PP variability with both time and discharge; these data were available only prior to April 2013, excluding the 2013–2017 time period from further consideration. The total annual PP load was highest in 2011 (15.1×10^3 t) and lowest in 2001 (0.63×10^3 t). Event contributions varied from 8.4% (2009) to 92.9% (2011), averaging 50.2 ± 0.23% on the annual scale. Averaged over 5 years, the average event contribution was 61.0 ± 15.1%. The 5-year total PP load was highest for 2008–2012 (20.9×10^3 t) and lowest for 1998–2002 (5.4×10^3 t). There were no obvious temporal patterns for the 1-year total PP

loads; 5-year total loads increased for all flows and event flows but had no consistent trend for non-event flows.

Observed daily PN concentrations varied from 0.001 mg/L (20 May 1997, 2 Apr 2003) to 7.6 mg/L (8 Sep 2011). Annual-average PN varied from 0.10 ± 0.05 mg/L (2009) to 0.70 ± 1.5 mg/L (2011) and showed a clear decrease over time, even including an anomalously high value in 2011. Annual-average PN also decreased over time for non-event flows but showed no consistent temporal trend for event flows, whether or not flows above the scour threshold were included. The 5-year average PN concentration significantly decreased for all flows and non-event flows. Five-year average PN significantly decreased for event flows but only when 2008–2012 was excluded ($p < 0.001$, $R^2 = 0.94$); this was also true for event flows below the scour threshold ($p < 0.001$, $R^2 = 0.89$). The annual average ratio of PN to river discharge significantly decreased over time for all flows and non-event flows but showed no evident temporal patterns for event flows, even after excluding large scour events as potential outliers. The 5-year average ratio had no consistent trends for all flows but declined significantly for non-events. Five-year average ratios decreased for events but only for those flows below the scour threshold. Only 14 PN observations were made during flows above the scour threshold.

Like PP, the wide variability of PN with river discharge precluded robust rating-curve calculations, and PN loads were calculated with WRTDS-derived concentrations (Zhang et al. 2015). The annual total PN load varied from 3.1×10^3 t in 1979 to 38.6×10^3 t in 2011. While there was no consistent linear trend over time, annual loads significantly increased from 1978 to 1996 ($p = 0.01$, $R^2 = 0.32$), had similar and low values until 2001, increased to 2004, then decreased to 2012. The post-2004 decrease is statistically significant if 2011 is excluded ($p = 0.03$, $R^2 = 0.65$). Events contributed an average of 41.8 ± 21.9% to the annual loads, highest in 2011 (90.7%) and lowest in 2008 (8.3%), with no apparent temporal trends. There was a significant increase in the 5-year total loads, with an average event contribution of 49.4 ± 16.8%. Event contributions generally increased over time, except for relatively low contributions in 1988–1992 and 1998–2002.

Particle Settling Velocities

The range of flows sampled for the direct settling velocity measurements was small, between 3030 and 4842 m^3/s. The range of suspended sediment concentrations (SSC) was larger, between 11 and 118 mg/L. While there was a tendency for SSC to increase with increasing flow, there was significant variability in SSC values at very similar flows, revealing the myriad other factors that affect instantaneous SSC. Mass fractions in different settling speed categories varied only slightly across all dates and locations sampled. There was a tendency for the fraction in the slowest settling category to decrease with increasing flow, accompanied by a slight increase in the mass fractions of the middle two settling categories. For the range of flows sampled, approximately 70% of the SSC settled slower than 0.01 mm/s, 25% settled between 0.01 and 0.2 mm/s, 4% settled between 0.2 and 2 mm/s, and 1% settled faster than 2 mm/s. Mass fraction estimates in different settling speed categories based on disaggregated particle sizes from simultaneous USGS samples were consistent with both Owen tube methods, tending to split any differences between them (Fig. S4). The settling velocity estimates using all three techniques were statistically indistinguishable, indicating that settling velocity estimates based on USGS disaggregated particle sizes under a broad range of flows are likely representative of actual settling velocity distributions. This in turn implies that particles passing through or over the Dam face are effectively disaggregated by the energetic turbulent flow conditions found there.

Based on the good agreement between our Owen tube settling experiments and the disaggregated particle size estimates of settling velocity at Conowingo, we used USGS National Water Information System (NWIS) data from Conowingo covering a much broader range of flows and dates to extend our analysis. Over the entire record, sampled flows ranged from 419 to 16,774 $m^3\ s^{-1}$, SSC from 13 to 2980 mg/L, and settling velocity distributions from almost entirely in the slowest settling category to more evenly distributed across categories at very high flows. Figure 5 summarizes observed changes in settling velocity distributions with increasing flow. Linear fits to the mass fraction in each category sum to 1 across all flows, as required to conserve mass. The trends of decreasing mass fraction with increasing flow in the slowest settling category and increasing mass fraction with flow in all other categories are much more apparent here than in our direct settling velocity measurements, primarily because the USGS particle-size data cover a much greater range of flows. Denoting each of these linear fits as f_i,

$$\begin{aligned} f_1 &= -1.938x10^{-5}Flow + 0.867 \\ f_2 &= 0.997x10^{-5}Flow + 0.116 \\ f_3 &= 0.773x10^{-5}Flow + 0.014 \\ f_4 &= 0.168x10^{-5}Flow + 0.003 \end{aligned} \quad (2)$$

These flow-dependent changes in mass fraction within different settling velocity classes were used directly in the numerical model to more accurately simulate suspended sediment input characteristics across a wide range of river flows.

Fate of Sediment in the Estuary

Sedimentology

Mud content of surficial sediments (uppermost 1 cm in cores) in the upper Bay generally increased downstream during the low-flow years 2015 ($p = 0.10$; $R^2 = 0.71$) and 2016 ($p > 0.10$). In contrast, mud content decreased with distance downstream after

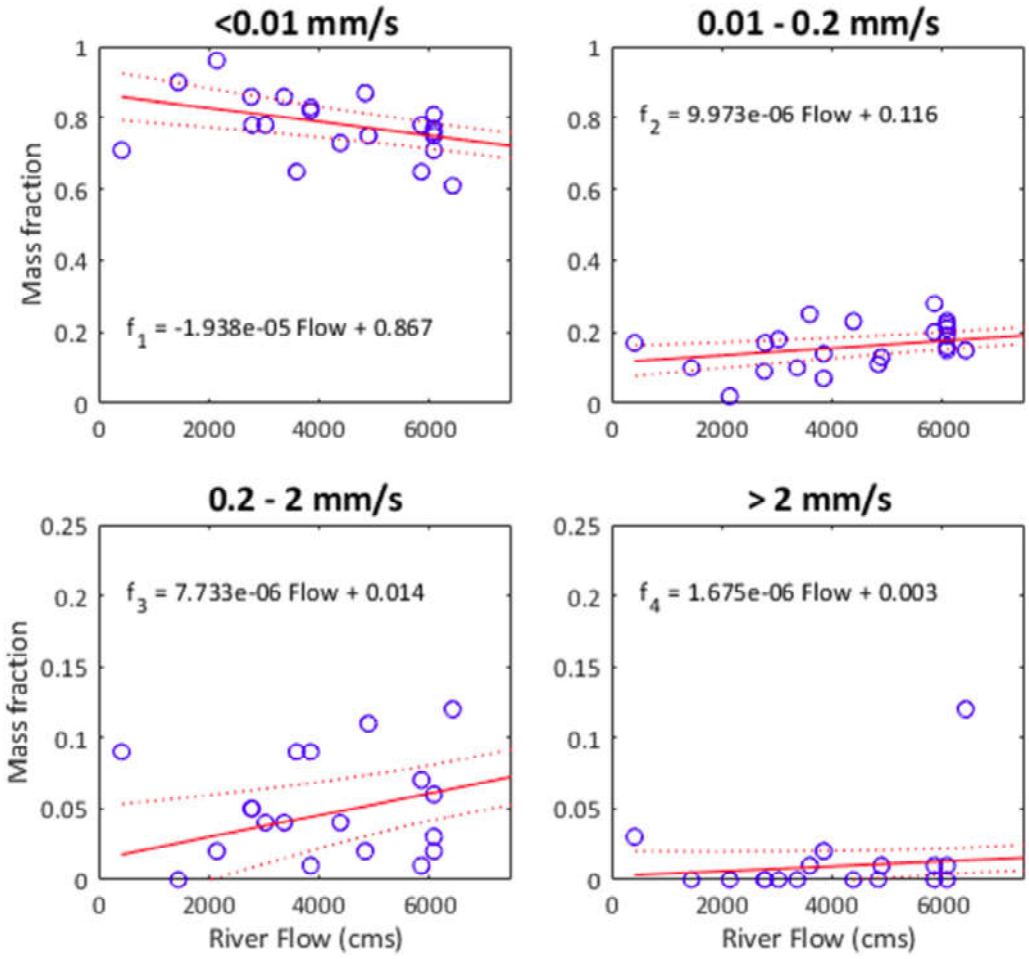

Fig. 5 Mass fractions in different settling velocity classes as a function of flow speed, from USGS particle size observations at Conowingo Dam. The linear least-squares fits for mass fraction in the different settling velocity classes sum to one across all river flows

TS Lee (Fig. 6a). Correspondingly, sediment at the most upstream site (Lee7; ~ 20 km from the Susquehenna River mouth; see Fig. 3) was much coarser after non-event flows (~ 60–70% mud) than after TS Lee (~ 90% mud), and sediment at the most downstream site (LeeS2; ~ 120 km from the Susquehanna River mouth) was much finer after non-event flows (nearly 100% mud) than after TS Lee (~85% mud). Averaged across sites sampled in all years ($n = 4$), average mud content was higher after TS Lee (89.9 ± 4.0%) than after non-event flows (lowest in 2015; 84.2 ± 14.1%), but the difference was not statistically significant. ^{7}Be inventories at each site indicate the amount of watershed sediment deposited within the previous 77–250 days (see "Methods"). While average sedimentation rates can be calculated by extrapolating the inventory over this time period, sediment likely was delivered relatively quickly after TS Lee but more gradually under non-event conditions. Inventories during 2015 and 2016 were highest at Lee2.5 (~ 55 km from the Susquehanna River mouth; Fig. 6b), but the maximum inventory after TS Lee occurred at Lee7 and decreased linearly downstream ($R^2 = 0.78$, $p = 0.005$). For the sites sampled in all years ($n = 4$), the average ^{7}Be inventory was highest after TS Lee (2.6 ± 2.1 dpm/cm^2) and lowest in 2016 (0.9 ± 0.7 dpm/cm^2); this difference was statistically significant ($p = 0.04$; paired t test). Thus, the most obvious differences between non-event and event flows occurred at the most up- and downstream sites, with much more deposition and finer sediments upstream, and less deposition and coarser sediments downstream, after TS Lee.

Over longer, decadal time scales, sediment accumulation rates were variable throughout the upper Bay, from 0.26 cm/year at LeeS2 to 1.2 cm/year at Lee5 (~ 30 km from the Susquehanna River mouth; Russ and Palinkas in review; Russ 2019). A precise accumulation rate could not be calculated for Lee2, because the regression fit required by the CFCS model was not statistically significant; instead the minimum rate of 0.81 cm/year was determined by noting the presence of excess ^{210}Pb (~ 100 year) at the base of the core (81 cm). At all other sites, regression models were statistically significant, implying dominance of steady-state sedimentation, rather than event sedimentation, over longer time scales. Down-core grain-size profiles were generally uniform, supporting the interpretation of steady-state sedimentation and also indicating that no major

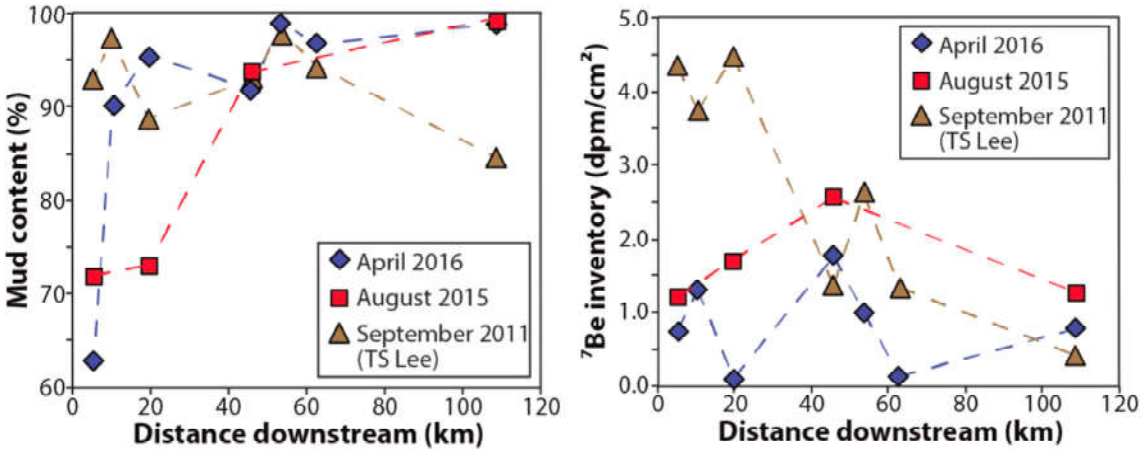

Fig. 6 **a** Mud content of surficial sediments and **b** total ^{7}Be inventories at sites in the upper Chesapeake Bay plotted versus distance downstream from Lee7 (arbitrarily set at 5 km) for 3 different time periods denoted by differing symbology

changes in sediment character have occurred in the upper Bay over the last ~100 y.

Transport Modeling

The COAWST model simulated sediment dynamics in Chesapeake Bay between 1 May 2015 and 30 June 2016, a ~ 1-year period that includes the time of field observations (August 2015, April 2016). The lack of event flows during this period, and the absence of major storms, resulted in trapping of most suspended sediments within the upper Bay around the ETM zone (Fig. 7). Nevertheless, there were clearly seasonal differences in SSC, with elevated SSC (10 mg/L) in the upper Bay during the 2016 spring freshet, as well as transport of small amounts of clay and silt to the mid-Bay. Ultimately, most fluvial sediments were deposited in the Susquehanna Flats, with thicknesses < 1 cm per month (Fig. 8).

Event conditions were simulated with hindcasts of TS Lee (2011) and Hurricane Ivan (2004), two recent flood events that had largest impacts on sediment loading into Chesapeake Bay. While previous work with TS Lee assumed fixed percentages of clay, silt, and sand (40%, 50%, and 10%, respectively; Cheng et al. 2013) for Susquehanna River sediment, this hindcast of TS Lee used flow-dependent percentages for the sediment classes from the observations (i.e., Fig. 5 and Table 1). While the total amount of flood-discharged sediment was unchanged (6.7×10^6 t), there were major differences in the size distribution of fluvial sediments. In Cheng et al. (2013), only 0.6×10^6 t of sand was discharged to the Bay versus 6.1×10^6 t of clay and fine silt. In contrast, the new model showed discharge of 1.5×10^6 t of coarse silt and sand, 2×10^6 t of fine silt, and 3.2×10^6 t of clay (Fig. S5). At these extreme river flows, larger amounts of coarser sediment components were scoured from the Reservoir bed and delivered to the Bay. The sediment plume after Hurricane Ivan showed a similar temporal evolution as that observed during TS

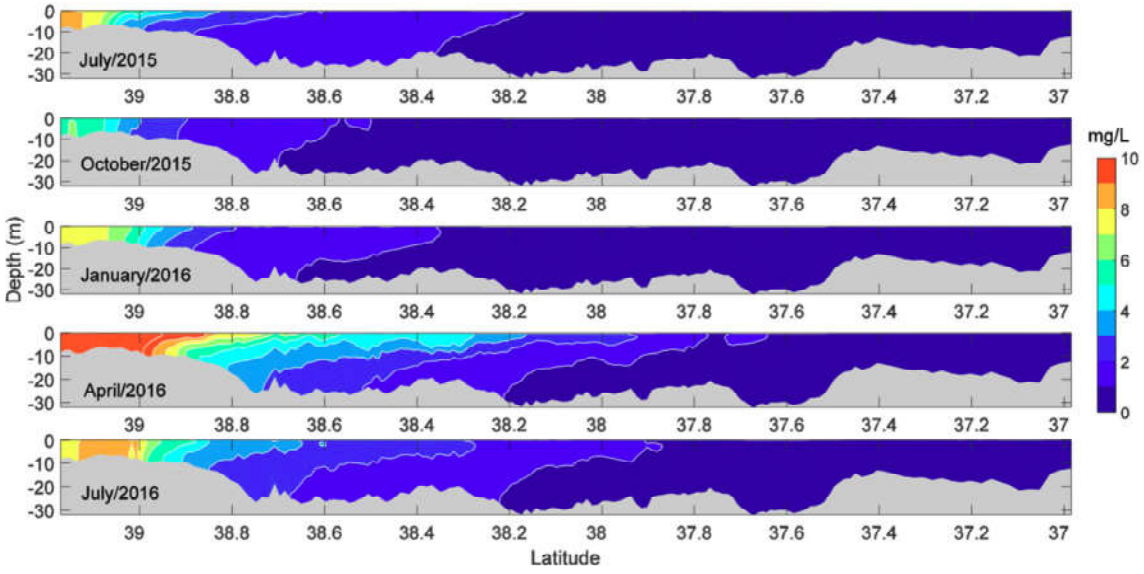

Fig. 7 Along-channel distribution of monthly averaged suspended sediment concentration under normal flow conditions experienced during the field campaigns

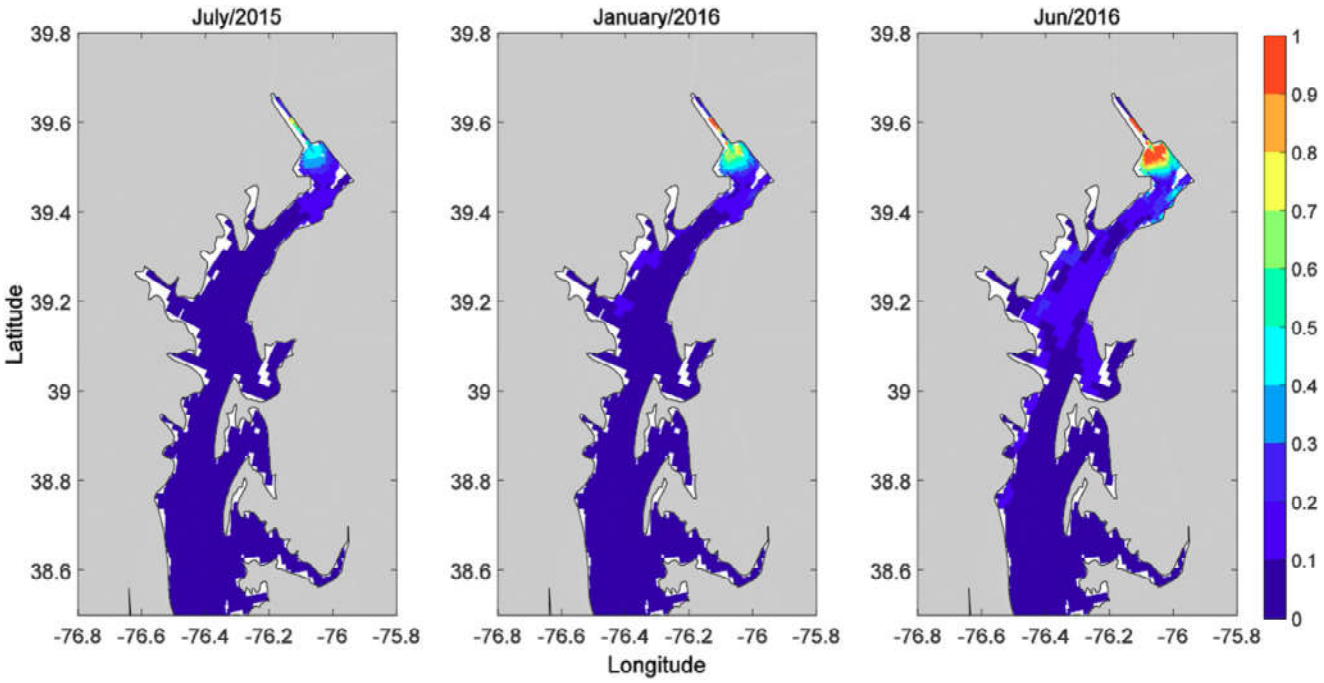

Fig. 8 Monthly average of thickness of sediment deposits (in cm) in the upper Bay for (left to right) July 2015, January 2016, and June 2016

Lee (not shown). Depositional patterns were also similar to TS Lee: most coarse silts and sands were deposited in the upper reaches of the Susquehanna Flats with a maximum thickness of 3 cm; fine silts were deposited everywhere in the upper Bay but with highest deposition (1 cm) in the Susquehanna Flats; clays were widely dispersed in the upper and mid-Bay regions with a thickness < 0.3 cm (Fig. S5). Although the processes of sediment transport and deposition were quite similar between Hurricane Ivan and TS Lee, the magnitude of sediment flux and deposition was quite different, responding non-linearly to Susquehanna River discharge. Peak discharge during TS Lee was ~ 1.5 times higher than during Hurricane Ivan (2.2×10^4 m^3/s for Lee; 1.5×10^4 m^3/s for Ivan), but the total sediment load delivered to the Bay was ~ 4.5 times higher after TS Lee than Hurricane Ivan (6.7×10^6 t for Lee; 1.5×10^6 t during Ivan) (Fig. S6). While part of this difference might be related to the longer flood duration for TS Lee, a more likely explanation is the nonlinearity of the loading curve.

Sediment Biogeochemistry and Exchange with Water Column

Sediment-Water Fluxes in the Reservoir and Estuary

The overall rates of sediment oxygen uptake (Fig. 9) within the three lower Susquehanna River Reservoirs and the upper Chesapeake Bay were compared in spring 2016. Because temperatures were changing rapidly, all rates were adjusted to 20 °C following Schnoor (1996). There were no significant differences between the stations within the Reservoir or between the Reservoir and the nearby upper Bay (Fig. 9). The sediment-water exchange of soluble reactive phosphorus was low and often directed into the sediment (Fig. S7). Overall, the dominant efflux of nitrogen was as N_2-N with ammonium showing highly variable rates and average nitrate plus nitrate concentrations directed into the sediment. In May of 2015, sediment-water NH_4^+ effluxes and NO_{23}^- influxes were elevated, but rates measured at all other times of year were small (Fig. S7).

Characterization of Sediment Composition and Reactivity

Rates of anaerobic ammonium production were generally low, with higher rates from fluvial sediments collected at the Dam outflow than observed from a survey of 13 sediment stations. Anaerobic nitrogen remineralization rates were determined from sediment and suspended sediments using time course incubations (Fig. 10). Observations from surficial sediments (0–2 cm depth) averaged 15% of rates from the water column. Long-term incubations of deeper sediments suggested extremely low rates of N remineralization, with the low rates making measurements difficult, even over the course of > 180 days of incubation. These rates reflect a mix of terrestrial and algal organic matter inputs and suggest that surficial sediments quickly lose much of their reactivity after deposition.

Biogeochemical Modeling

Biogeochemical model simulations and diagenesis experiments indicated that depositing organic material in the

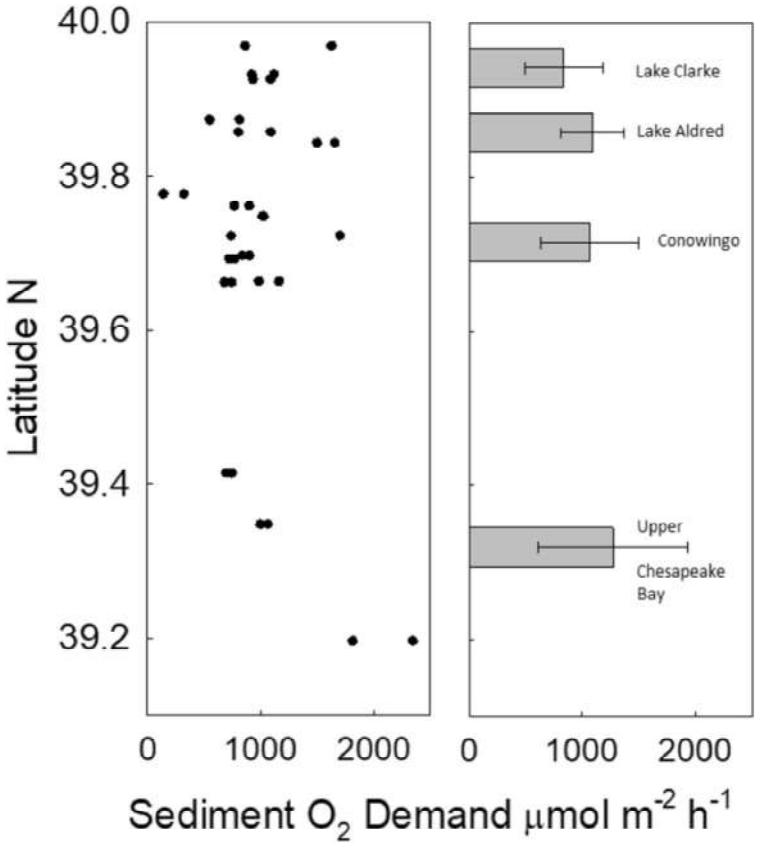

Fig. 9 Sediment oxygen demand as a function of latitude, including upper bay sediments and all 3 reservoirs in the lower Susquehanna River. The data were all collected in April 2016, with temperatures of 9.6 °C in Conowingo Reservoir, 14.5 °C in the upper Chesapeake Bay, and to 18 °C in Lake Clarke and Lake Aldred. All plotted data were adjusted to 20 °C following Schnoor (1996) to allow a more direct comparison. The error bars represent standard deviation and there was no significant difference in the different segments

Conowingo Reservoir has moderate/low reactivity relative to phytoplankton-derived organic material (26% G1; 20% in G2; 54% in G3 in Reservoir versus 65% G1; 20% G2 and 15% G3 for phytoplankton) and that 94% of the sediments that accumulate in the Reservoir were refractory. Consequently, sediment-water fluxes of dissolved inorganic nitrogen and phosphorus were low and contributed a small fraction (< 0.1%) of the export flux of nitrogen and phosphorus from the Reservoir (Fig. S7). Using model-derived estimates of sediment P and N content of the sediment and assuming that scour could remove either the top 5 cm or 10 cm of the sediment, the potential relative contribution of scoured reservoir sediments to this export flux during events is much higher for phosphorus than for nitrogen. For phosphorus, scouring bottom sediments to a depth of 10 cm would represent 131% of the annual TP export from the Reservoir, while for nitrogen, it would account for only 7.3%. This reservoir scour estimate is half of the TP load delivered during TS Lee, but only 12% of the TS Lee TN input.

The potential biogeochemical impact of depositing scoured Reservoir sediments in the upper Bay was explored via numerical experiments. Specifically, the sensitivity of sediment-water fluxes to altered deposition rates and composition of depositing organic material (scoured Reservoir sediments versus more typical phytoplankton detritus) was tested (see "Methods"). While changes in deposition rates yielded expected proportional changes in sediment C:N:P content and sediment-water fluxes (Fig. 11), increased deposition rates only resulted in better representation of dissolved O_2 fluxes. In addition, while all three simulations represented sediment nitrogen content well (model = 0.19 %N, data =

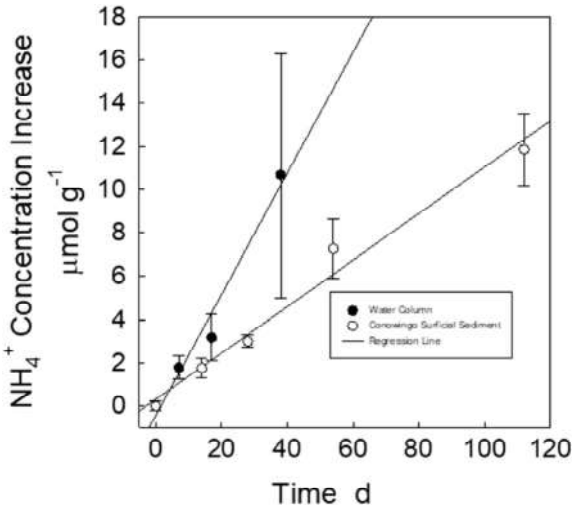

Fig. 10 Plot of ammonium concentrations on a dry mass basis for 16 anaerobic sediment incubations from May 2015 and 7 anaerobic water-column incubations from February 2016. The error bars are standard errors, and the slopes are 0.05 and 0.223 μmol g^{-1} day^{-1} for sediment and water column

0.23 ± 0.05 %N), they under-predicted %C (model = 1.9, data = 3.9 ± 1.3), and over-predicted %P (model = 0.14, data = 0.06 ± 0.02). We also compared three simulations with different formulations for the estimated organic matter deposition rates. In addition to the "Base" scenario, we deposited the same organic material as in the "Base" case but with reactivity fractions matching the Conowingo simulation; we also estimated organic-matter deposition rates from overlying-water chlorophyll-a, which has increased slightly over time (Fig. 11). These simulations revealed that dissolved O_2 and ammonium fluxes were better represented by the chlorophyll-a based deposition rates, but that phosphorus pools and sediment-water fluxes were overestimated (Fig. 11).

Synthesis of recent sediment-water fluxes measurements with historic observations indicates that sediment-water fluxes of nitrogen and phosphorus in the Conowingo Reservoir are similar to upper Chesapeake Bay and are low relative to mesohaline Bay sediments. Measurements made in 2015 indicate that sediment-water P fluxes in the Conowingo Reservoir and upper Bay typically range from low rates of net uptake (~− 15 μmol P m^{-2} h^{-1}) to low levels of net release (~ 2–15 μmol P m^{-2} h^{-1}), compared to warm-season maxima of 30–90 μmol P m^{-2} h^{-1}at low-oxygen, mid-Bay stations (Testa et al. 2013). Similarly, recently observed ammonium fluxes range from 0 to 600 in the Conowingo and Upper Bay (with the majority of fluxes < 200 μmol N m^{-2} h^{-1}, compared to rates consistently in the range of 300–800 μmol N m^{-2} h^{-1}at low-oxygen, mid-Bay stations (Brady et al. 2013). While the low N and P fluxes typical of upper Bay and Reservoir sediments have been measured in shallower, well-oxygenated sediments, these sediment-water flux rates are elevated in adjacent deeper sediments, which cover a limited area in the upper Chesapeake Bay (Boynton and Rohland 1998). Clearly, despite consistently high deposition rates in these low-salinity regions of Chesapeake Bay and the upstream Conowingo Reservoir (see above), the sediments in these habitats efficiently retain nutrients.

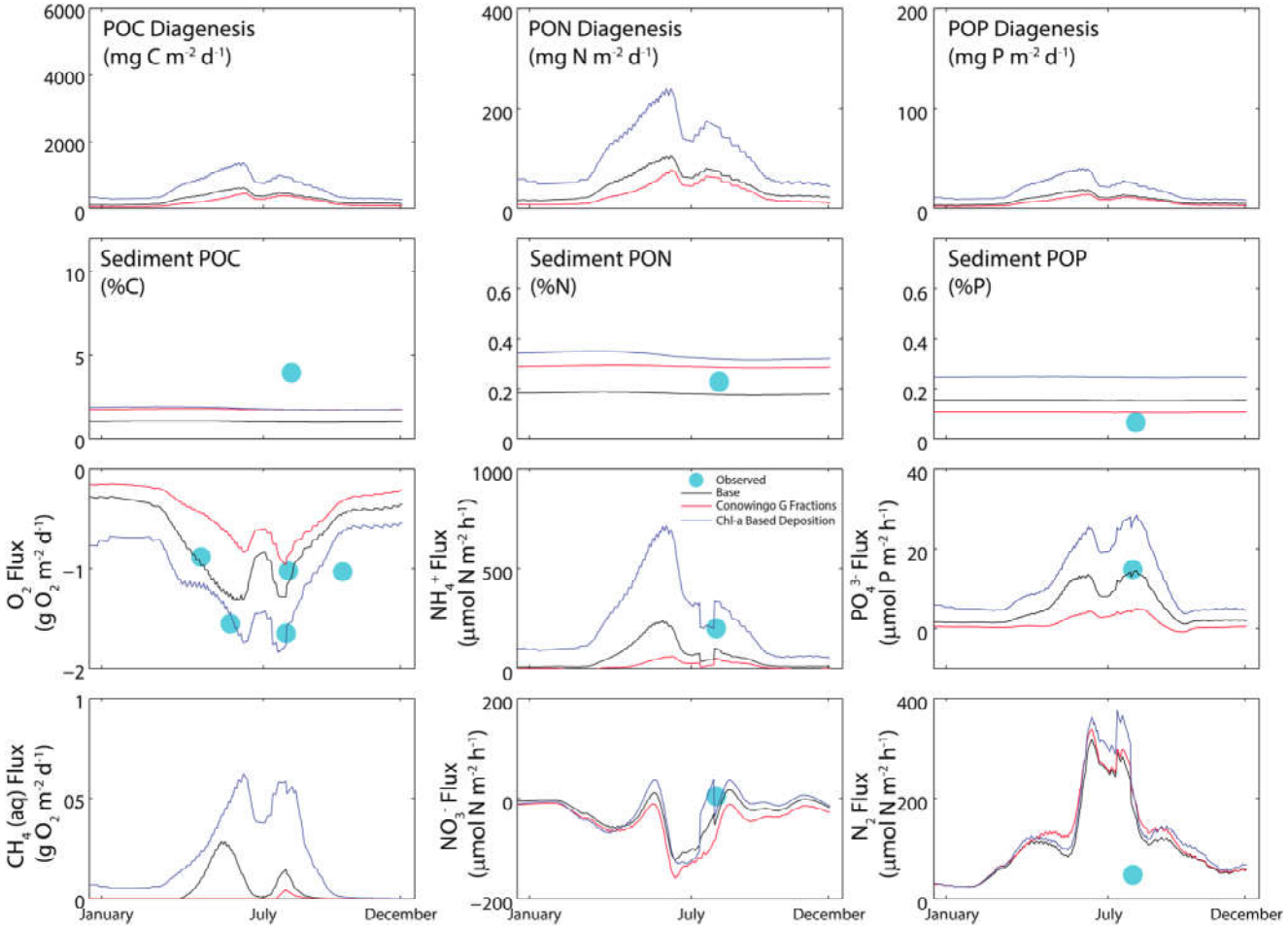

Fig. 11 Modeled (lines) and/or observed (circles) diagenesis rates, sediment carbon/nutrient content, and sediment-water fluxes for the year 2015 under the baseline simulation (black lines; Brady et al. 2013), a simulation based upon the baseline POM deposition rates but with Conowingo Reservoir sediment-like material (red lines; G1 = 0.26, G2 = 0.2, G3 = 0.54), and deposition calculated from algal G fractions and observed water-column chlorophyll-a time-series (blue lines; G1 = 0.65, G2 = 0.2, G3 = 0.15)

Discussion

This paper synthesizes data from a variety of methods, each of which have their own limitations and uncertainties (see "Methods" and Fig. 1). However, all of these data resulted from a coordinated interdisciplinary study, such that observations and model results represent similar spatial and temporal scales. For example, sedimentological and biogeochemical field sampling was simultaneous in the upper Bay, and transport and biogeochemical modeling covers the period of these observations. Additional transport-model runs for 2004 and 2011 captured event conditions that were not present during the field study. The 2011 model run is the same as Cheng et al. (2013), but with updated parameterization provided by the particle-settling velocity experiments, and compared to field observations of the same event by Palinkas et al. (2014). Because we were interested in changes over time, we obtained river discharge and suspended-constituent data for as many years as possible. We chose to run these analyses through 2017 to have 4 full decades of data. The sediment biogeochemical model was run from 1985 to 2015 to validate the model against observations made at various times over the past three decades; analysis of model output focuses on 2015 when most contemporary observations were made. As such, the dataset for this paper is unique in its spatial and temporal scope, capturing physical and biogeochemical processes along the entire river-estuary continuum. In particular, these data reveal that the character and magnitude of particulate dynamics throughout the Susquehanna River-upper Chesapeake Bay continuum are quite different for non-event and event flows. Thus, it is useful to consider the two conditions separately.

Non-event Flows

Non-event flows occur most of the time, ~90% of the days since 1978, and thus represent "every-day" conditions. In the reservoir, sediment deposition is driven by a balance of sediment supply and physical energy, following expectations from most river-delta systems and reservoirs around the world (Alexander et al. 1991; Pirmez et al. 1998; Palinkas 2009). In particular, most sediment delivered at the upstream reservoir boundary remains in suspension due to higher physical energy and is transported to the more quiescent middle region, where it can rapidly deposit. Near the downstream boundary, sediment supply has been depleted and the energy is likely higher due to the Dam turbines, inhibiting deposition. Suspended sediment and attached nutrients are thus transported over the Dam and are largely composed of watershed material, since flows are typically well below any estimates of the scour threshold.

Suspended-sediment, and attached phosphorus and nitrogen, loads delivered to the Bay past Conowingo have declined since 1978 for equivalent non-event river flows. This decrease occurred even though river discharge on the same subset of days increased and likely reflects impacts of BMPs in the watershed. For the Susquehanna, most trend analyses of loads since the 1980s indicate increasing loading of particulate forms of N and P (Hirsch 2012; Zhang et al. 2013), but these studies include all river flows together. For the low, non-event flows that occur most of the time, our analyses show just the opposite—decreasing loads over time that likely reflect efforts in the watershed to reduce these loads through BMP installation.

Event Flows

Event flows are stochastic and have significant, non-linear effects on river discharge, sediment dynamics, and geochemistry. In the Reservoir, event flows redistribute sediment, eroding temporary stores from channels and the mid-Reservoir region and transporting them downstream near the Dam, which facilitates net accumulation by its physical presence, and over the Dam into the upper Bay. Flows that exceed the scour threshold are particularly effective at delivering large amounts of Reservoir sediment to the upper Bay, and there is currently much interest in defining the threshold value. The often-cited 400,000 cfs (11,326.7 m^3/s) value originated from Gross et al. (1978), cited by Lang (1982), and was based on a 1-year comparison of sediment loads at Harrisburg (PA, upstream of the Marietta gauge) and Conowingo, assuming that the threshold occurs when loads at Harrisburg are lower than at Conowingo. This comparison necessarily assumed no sediment inputs/outputs between these two gauges, ignoring several small tributaries and perhaps more importantly the two reservoirs upstream of Conowingo. More recent work suggests that the scour threshold has decreased with Reservoir infill and now could be as low as 175,000 cfs (4955.4 m^3/s; Hirsch 2012).

Our analyses of event flows between the typical opening of the first flood gate at 86,400 cfs (2446.5 m^3/s) and 400,000 cfs showed increasing amounts of suspended materials for an equivalent river discharge over time, consistent with a decreasing scour threshold. However, there is another effect of reservoir infill that has received much less attention—decreasing deposition of watershed sediment as it passes through the reservoir. Decreasing deposition accompanies infilling because the decrease in cross-sectional area due to infilling increases flow speed and bottom stress, which keeps sediment in suspension. Both a lower scour threshold and decreasing deposition are likely active and drive the observed increased in suspended loads during moderately large flows. Event flows > 400,000 cfs occur infrequently (every ~5–7 years), and have few observations of SSC and particulate nutrients (n~15 for the entire 1978–2017 period), preventing robust trend analyses.

Recent attention has been focused on the potential impacts on Chesapeake Bay of elevated particulate N and P inputs associated with more frequent scour events within the Conowingo Reservoir (e.g., Cerco 2016). Our synthesis suggests that the potential biogeochemical impacts of these elevated inputs are limited in time and space for several reasons. First, despite the fact that scour events likely occur even more frequently than indicated by the 400,000 cfs scour threshold, model analyses of reservoir sediments suggest that a substantial scour event (top 5 cm of the entire reservoir) would contribute 20% of P loads in a TS Lee-like storm and only 6% of N loads. The scoured particulate N and P loads that do enter the Chesapeake Bay are also highly refractory (turnover time » 1 year). Second, particulate forms of N and P that enter Chesapeake Bay are efficiently retained in the upper Bay, especially near the Susquehanna River mouth, due to high sinking rates or trapping within the ETM (Sanford et al. 2001). Our finding that delivered particles coarsen and associated settling speeds increase as flow rates increase further amplifies upper Bay sediment trapping. Third, the tidal fresh/oligohaline region where the majority of sediments deposit has typically low rates of sediment-water N and P fluxes, as a result of high rates of denitrification (Testa et al. 2013), effective phosphorus retention in iron-enriched, oxidized sediments (Hartzell et al. 2017), and low reactivity of the organic material (Fig. 10). Furthermore, any scoured material that is regenerated in the upper Bay enters a highly enriched water column that is rarely nutrient limited (Fisher et al. 1999). Consequently, model simulations of scour events within Conowingo Reservoir have only shown marginal impacts on dissolved oxygen (Cerco 2016).

Over longer, decadal time scales, event sediments in this region are effectively redistributed such that their signal is not obvious in sediment cores. However, unlike non-event flows, event flows are capable of transporting fine sediment downstream of the ETM as evidenced by model results and preservation of event-sediment signatures in cores. When sediment reaches the mid-Bay region, it encounters saltier, mesohaline waters that in the Chesapeake ecosystem are typically hypoxic or anoxic during summer (Testa and Kemp 2014). Low oxygen conditions, in combination with high concentrations of sulfate that eventually lead to sulfide accumulation, allow for high rates of sediment-water efflux of phosphorus and ammonium, especially during warm months (Cowan and Boynton 1996; Testa and Kemp 2012). While we do not have model simulations or measurements to track the potential relocation of particulate nutrients from their initial deposition in the upper Bay to more seaward waters, prior analysis in mesohaline Chesapeake Bay sediments has shown clear relationships between recently deposited chlorophyll-a and N and P fluxes (Cowan and Boynton 1996), indicating that local phytoplankton production drives these fluxes.

It is important to keep in mind that, while events can deliver enormous amounts of sediment to the Bay, they occur infrequently (~ 10% of the time). Moreover, sediment deposition in the mesohaline region is relatively small in magnitude (e.g., only ~ 1 cm after TS Lee), minimizing potential impacts to Bay biogeochemistry. In fact, the Bay has been remarkably resilient to recent storm events. For example, SAV beds in the upper Bay experienced some erosion during TS Lee but were able to mostly withstand the event (Gurbisz et al. 2016). In the years following, most indicators of Bay health show improving water quality and expansion of SAV in low-salinity regions (Lefcheck et al. 2018; Testa et al. 2018; Zhang et al. 2018). However, note that no other large events occurred after TS Lee until July 2018 when the Susquehanna River at Conowingo crested at 376,000 cfs (10,647.1 m^3/s; https://waterdata.usgs.gov/nwis). Between those two events, the highest flow (except for 1 day in Feb 2013) was during the 2017 spring freshet when the highest flow was 177,870 cfs (5036.7 m^3/s; https://waterdata.usgs.gov/nwis). This gap between large events likely aided the Bay's recovery, similar to the string of dry years that likely aided recovery of SAV on the Susquehanna Flats (Gurbisz and Kemp 2014).

Prior investigations into the impacts of reservoir construction on the transport of material to the coastal zone and the subsequent response have often differed from our discussion of the lower Susquehanna River reservoirs. While the primary problem identified with the infilling of Conowingo Reservoir is the potential *increase* in particulate nutrient inputs, the focus of other studies has often examined dam impacts on nutrient load *reductions*. In part, this discrepancy reveals the contrast between reduced sediment trapping in mature reservoirs (Conowingo) versus increased sediment trapping in young reservoirs. For example, the once highly productive fisheries of Mediterranean waters near the outflow of the Nile River appeared to degrade after the construction of the Aswan Dam, which severely reduced riverine sediment and nutrient inputs (Nixon 2003), but fisheries recovered once anthropogenic nutrient inputs increased. The construction of the Three Gorges Dam on the Yangtze River reduced the silica to nitrogen ratio and nutrient inputs overall, which was associated with phytoplankton productivity declines in the East China Sea (Gong et al. 2006). Long-term reductions in the silica to nitrogen ratio have been described for other large rivers (e.g., Mississippi; Turner and Rabalais 1991), and in some cases, these altered rations have been associated with reduced diatom productivity (e.g., Danube River and Northwestern Black Sea; Humborg et al. 1997). Thus, the nature of the history and geology of a given dam (age, trapping capacity) is critical to understanding its role in the productivity and biogeochemistry of receiving waters.

Conclusions

This study synthesized field observations, model results, and long-term monitoring data along the reservoir-estuary continuum to evaluate potential impacts of Conowingo Reservoir infilling on Chesapeake Bay biogeochemistry (see Fig. 1). Results show that, for equvialent river discharges, sediment loading has decreased during non-event flows but increased during event flows (question 1 in the Introduction). The potential biogeochemical impacts of these elevated inputs is limited, because scoured particulate nitrogen (N) and phosphorus (P) loads that do enter the Bay are highly refractory (turnover time » 1 year) and would contribute a relatively small fraction of loading in an extreme storm like Tropical Storm Lee (question 2). Also, these sediments are efficiently retained in the upper Bay due to high sinking rates or trapping in the ETM but can be transported downstream during events (question 3). Thus, while large precipitation and riverine flow events are significant and can generate a substantial short-term impact on receiving waters in Chesapeake Bay, the estuary is remarkably resilient to storms (question 4). This recovery potential is likely aided by long time lags between major events and an underlying improvement in watershed management that is evident during low flow periods. The maturation of dams (i.e., infilling) over time shifts these constructed ecosystems from net nutrient and sediment sinks to sources, which changes their effect on downstream waters from that of a nutrient and sediment sink to that of a source. The Chesapeake Bay will be negatively influenced by continued infilling of reservoirs and the loss of an unintended watershed BMP, but the scale of the potential impact of elevated particulate nutrient inputs on the mainstem Chesapeake Bay is likely small compared to ongoing reductions in dissolved nitrogen and phosphorus in many regions of the watershed.

Acknowledgments The authors thank the many colleagues, students, and technicians who made this work possible. In particular, we thank USGS colleagues Michael Langland and Joel Bloomquist, as well as Majorie Zeff from AECOM. We thank Debbie Hinkle and Mike Owens for invaluable field and lab assistance. Emily Russ, Stephanie Barletta, and Zoe Vulgaropulos were graduate students at Horn Point Lab supported by this project and contributed many insights from their theses to this work. Casey Hodgkins contributed to sediment biogeochemical model simulations, data analysis, and preparation of Fig. 2.

Funding Information The authors of this paper were supported by grants from Maryland Sea Grant (from the National Oceanic and Atmospheric Administration, U.S. Department of Commerce award NA14OAR4170090 to Sanford and Palinkas; award NA14OAR4170090 SA75281450-G to Cornwell), the Grayce B. Kerr Fund (to C. Palinkas), and Exelon through the Maryland Department of Natural Resources (107C04105 to all authors). This is UMCES contribution number 5651.

References

Alexander, C.R., D.J. DeMaster, and C.A. Nittrouer. 1991. Sediment accumulation in a modern epicontinental-shelf setting: The Yellow Sea. *Marine Geology* 98 (1): 51–72. https://doi.org/10.1016/0025-3227(91)90035-3.

Appleby, P.G., and F. Oldfield. 1978. The calculation of lead-210 dates assuming a constant rate of supply of unsupported ^{210}Pb to the sediment. *Catena* 5 (1): 1–8. https://doi.org/10.1016/S0341-8162(78)80002-2.

Barmawidjaja, D.M., G.J. van der Zwaan, F.J. Jorissen, and S. Puskaric. 1995. 150 years of eutrophication in the northern Adriatic Sea: Evidence from a benthic foraminiferal record. *Marine Geology* 122 (4): 367–384. https://doi.org/10.1016/0025-3227(94)00121-Z.

Bayley, S., V.D. Stotts, P.F. Springer, and J. Steenis. 1978. Changes in submerged aquatic macrophyte populations at the head of Chesapeake Bay, 1958-1975. *Estuaries* 1 (3): 171–182. https://doi.org/10.2307/1351459.

Biggs, R.B. 1970. Sources and distribution of suspended sediment in northern Chesapeake Bay. *Marine Geology* 9 (3): 187–201. https://doi.org/10.1016/0025-3227(70)90014-9.

Booij, N., R.C. Ris, and L.H. Holthuijsen. 1999. A third-generation wave model for coastal regions: 1. Model description and validation. *Journal of Geophysical Research, Oceans* 104 (C4): 7649–7666. https://doi.org/10.1029/98JC02622.

Boynton, W.R., and F.M. Rohland. 1998. Sediment-water flux status and trends: 1997 Patuxent River study. In Maryland Chespeake Bay water quality monitoring program ecosystem processes component level one report #15 interpretive report, 71–217.

Boynton, W.R., L. Lubbers, K.V. Wood, and C.W. Keefe. 1984. *Seston dynamics in the lower Susquehanna River. Final data report to Martin Marietta Corporation [UMCES]CBL 84–81*. Solomons, MD: University of Maryland Center for Environmental Science.

Boynton, W.R., J.H. Garber, R. Summers, and W.M. Kemp. 1995. Inputs, transformations, and transport of nitrogen and phosphorus in Chesapeake Bay and selected tributaries. *Estuaries* 18 (1): 285–314.

Brady, D.C., J.M. Testa, D.M. Di Toro, W.R. Boynton, and W.M. Kemp. 2013. Sediment flux modeling: Calibration and application for coastal systems. *Estuarine, Coastal and Shelf Science* 117: 107–124. https://doi.org/10.1016/j.ecss.2012.11.003.

Brookes, A., K.J. Gregory, and F.H. Dawson. 1983. An assessment of river channelization in England and Wales. *Science of the Total Environment* 27 (2-3): 97–111. https://doi.org/10.1016/0048-9697(83)90149-3.

Brush, G.S. 1989. Rates and patterns of estuarine sediment accumulation. *Limnology and Oceanography* 34 (7): 1235–1246.

Brush, G.S. 2001. Natural and anthropogenic changes in Chesapeake Bay during the last 1000 years. *Human and Ecological Risk Assessment* 7 (5): 1283–1296. https://doi.org/10.1080/20018091095005.

Brush, G.S. 2009. Historical land use, nitrogen, and coastal eutrophication: A paleoecological perspective. *Estuaries and Coasts* 32 (1): 18–28. https://doi.org/10.1007/s12237-008-9106-z.

Burdige, D.J. 1991. The kinetics of organic matter mineralization in anoxic marine sediments. *Journal of Marine Research* 49 (4): 727–761. https://doi.org/10.1357/002224091784995710.

Cerco, C.F. 2016. Conowingo reservoir sedimentation and Chesapeake Bay: State of the science. *Journal of Environmental Quality* 45 (3): 882. https://doi.org/10.2134/jeq2015.05.0230.

Cerco, C.F., S.-C. Kim, and M.R. Noel. 2013. Management modeling of suspended solids in the Chesapeake Bay, USA. *Estuarine, Coastal and Shelf Science* 116: 87–98. https://doi.org/10.1016/j.ecss.2012.07.009.

Cheng, P., M. Li, and Y. Li. 2013. Generation of an estuarine sediment plume by a tropical storm. *Journal of Geophysical Research, Oceans* 118 (2): 856–868. https://doi.org/10.1002/jgrc.20070.

Coakley, J.P., and J.P.M. Syvitski. 1991. SediGraph technique. In Principles, methods, and application of particle size analysis, 129–142.

Cornwell, J.C., and P.A. Sampou. 1995. Environmental controls on iron sulfide mineral formation in a coastal plain estuary. In *Geochemical Transformations of Sedimentary Sulfur*, ed. M. A. Vairavamurthy and M. A. A. Schoonen, 224–242.

Cornwell, J.C., P.M. Glibert, and M.S. Owens. 2014. Nutrient fluxes from sediments in the San Francisco Bay delta. *Estuaries and Coasts* 37 (5): 1120–1133. https://doi.org/10.1007/s12237-013-9755-4.

Cowan, J.L.W., and W.R. Boynton. 1996. Sediment-water oxygen and nutrient exchanges along the longitudinal axis of Chesapeake Bay: Seasonal patterns, controlling factors and ecological significance. *Estuaries* 19 (3): 562. https://doi.org/10.2307/1352518.

Cronin, T.M., G.S. Dwyer, T. Kamiya, S. Schwede, and D.A. Willard. 2003. Medieval warm period, little ice age and 20th century temperature variability from Chesapeake Bay. *Global and Planetary Change* 36 (1-2): 17–29. https://doi.org/10.1016/S0921-8181(02)00161-3.

Donoghue, J.F., O.P. Bricker, and C.R. Olsen. 1989. Particle-borne radionuclides as tracers for sediment in the Susquehanna River and Chesapeake Bay. *Estuarine, Coastal and Shelf Science* 29 (4): 341–360. https://doi.org/10.1016/0272-7714(89)90033-4.

Edwards, R.E. 2006. *Comprehensive analysis of the sediments retained behind hydroelectric dams of the lower Susquehanna River*. 239. Watershed assessment and Protectio program Susquehanna River basin commission.

Elliott, A.J. 1978. Observations of the meteorologically induced circulation in the Potomac estuary. *Estuarine and Coastal Marine Science* 6 (3): 285–299. https://doi.org/10.1016/0302-3524(78)90017-8.

Fan, J., and G.L. Morris. 1992. Reservoir sedimentation. I: Delta and density current deposits. *Journal of Hydraulic Engineering* 118 (3): 354–369. https://doi.org/10.1061/(ASCE)0733-9429(1992)118:3(354.

Feddersen, F., M. Olabarrieta, R.T. Guza, D. Winters, B. Raubenheimer, and S. Elgar. 2016. Observations and modeling of a tidal inlet dye tracer plume. *Journal of Geophysical Research, Oceans* 121 (10): 7819–7844. https://doi.org/10.1002/2016JC011922.

Fisher, T.R., A.B. Gustafson, K. Sellner, R. Lacouture, L.W. Haas, R.L. Wetzel, R. Magnien, D. Everitt, B. Michaels, and R. Karrh. 1999. Spatial and temporal variation of resource limitation in Chesapeake Bay. *Marine Biology* 133 (4): 763–778. https://doi.org/10.1007/s002270050518.

Ganju, N.K., D.H. Schoellhamer, and B.E. Jaffe. 2009. Hindcasting of decadal-timescale estuarine bathymetric change with a tidal-timescale model. *Journal of Geophysical Research* 114 (F4). https://doi.org/10.1029/2008JF001191.

García-Robledo, E., A. Corzo, and S. Papaspyrou. 2014. A fast and direct spectrophotometric method for the sequential determination of nitrate and nitrite at low concentrations in small volumes. *Marine Chemistry* 162: 30–36. https://doi.org/10.1016/j.marchem.2014.03.002.

Gelfenbaum, G., A.W. Stevens, I. Miller, J.A. Warrick, A.S. Ogston, and E. Eidam. 2015. Large-scale dam removal on the Elwha River, Washington, USA: Coastal geomorphic change. *Geomorphology* 246: 649–668. https://doi.org/10.1016/j.geomorph.2015.01.002.

Gong, G.-C., J. Chang, K.-P. Chiang, T.-M. Hsiung, C.-C. Hung, S.-W. Duan, and L.A. Codispoti. 2006. Reduction of primary production and changing of nutrient ratio in the East China Sea: Effect of the three gorges dam? *Geophysical Research Letters* 33 (7). https://doi.org/10.1029/2006GL025800.

Gregory, K.J. 2006. The human role in changing river channels. *Geomorphology* 79 (3-4): 172–191. https://doi.org/10.1016/j.geomorph.2006.06.018.

Gross, M.G., M. Karweit, W.B. Cronin, and J.R. Schubel. 1978. Suspended sediment discharge of the Susquehanna River to northern Chesapeake Bay, 1966 to 1976. *Estuaries* 1 (2): 106. https://doi.org/10.2307/1351599.

Gurbisz, C., and W.M. Kemp. 2014. Unexpected resurgence of a large submersed plant bed in Chesapeake Bay: Analysis of time series data. *Limnology and Oceanography* 59 (2): 482–494. https://doi.org/10.4319/lo.2014.59.2.0482.

Gurbisz, C., W.M. Kemp, L.P. Sanford, and R.J. Orth. 2016. Mechanisms of storm-related loss and resilience in a large submersed plant bed. *Estuaries and Coasts* 39 (4): 951–966. https://doi.org/10.1007/s12237-016-0074-4.

Hagy, J.D., W.R. Boynton, C.W. Keefe, and K.V. Wood. 2004. Hypoxia in Chesapeake Bay, 1950–2001: Long-term change in relation to nutrient loading and river flow. *Estuaries* 27 (4): 634–658. https://doi.org/10.1007/BF02907650.

Haidvogel, D.B., H.G. Arango, K. Hedstrom, A. Beckmann, P. Malanotte-Rizzoli, and A.F. Shchepetkin. 2000. Model evaluation experiments in the North Atlantic Basin: Simulations in nonlinear terrain-following coordinates. *Dynamics of Atmospheres and Oceans* 32 (3-4): 239–281. https://doi.org/10.1016/S0377-0265(00)00049-X.

Hainly, R.A., L.A. Reed, H.N. Flippo, and G.J. Barton. 1995. Deposition and simulation of sediment transport in the lower Susquehanna River reservoir system. US Department of the Interior, US Geological Survey.

Harris, C.K., C.R. Sherwood, R.P. Signell, A.J. Bever, and J.C. Warner. 2008. Sediment dispersal in the northwestern Adriatic Sea. *Journal of Geophysical Research* 113 (C11). https://doi.org/10.1029/2006JC003868.

Hartzell, J.L., T.E. Jordan, and J.C. Cornwell. 2017. Phosphorus sequestration in sediments along the salinity gradients of Chesapeake Bay subestuaries. *Estuaries and Coasts* 40 (6): 1607–1625.

Hirsch, R.M. 2012. Flux of nitrogen, phosphorus, and suspended sediment from the Susquehanna River basin to the Chesapeake Bay during tropical storm Lee, September 2011, as an indicator of the effects of reservoir sedimentation on water quality. US Department of the Interior, US Geological Survey.

Hobbs, C.H., J.P. Halka, R.T. Kerhin, and M.J. Carron. 1992. Chesapeake Bay sediment budget. *Journal of Coastal Research* 8: 292–300.

Hudson, P.F., H. Middelkoop, and E. Stouthamer. 2008. Flood management along the lower Mississippi and Rhine Rivers (the Netherlands) and the continuum of geomorphic adjustment. *Geomorphology* 101 (1-2): 209–236. https://doi.org/10.1016/j.geomorph.2008.07.001.

Humborg, C., V. Ittekkot, A. Cociasu, and B.V. Bodungen. 1997. Effect of Danube River dam on Black Sea biogeochemistry and ecosystem structure. *Nature* 386 (6623): 385–388. https://doi.org/10.1038/386385a0.

Ibàñez, C., N. Prat, and A. Canicio. 1996. Changes in the hydrology and sediment transport produced by large dams on the lower Ebro river and its estuary. *Regulated Rivers: Research & Management* 12 (1): 51–62. https://doi.org/10.1002/(SICI)1099-1646(199601)12:1<51::AID-RRR376>3.0.CO;2-I.

Kana, T.W., C. Darkangelo, M.D. Hunt, J.B. Oldham, G.E. Bennett, and J.C. Cornwell. 1994. Membrane inlet mass spectrometer for rapid high-precision determination of N_2, O_2, and Ar in environmental water samples. *Analytical Chemisty* 66 (23): 4166–4170.

Kaste, J.M., S.A. Norton, and C.T. Hess. 2002. Environmental chemistry of Beryllium-7. *Reviews in Mineralogy and Geochemistry* 50 (1): 271–289. https://doi.org/10.2138/rmg.2002.50.6.

Kemp, W.M., R.R. Twilley, J.C. Stevenson, W.R. Boynton, and J.C. Means. 1983. The decline of submerged vascular plants in upper Chesapeake Bay: Summary of results concerning possible causes. *Marine Technology Society Journal* 17: 78–89.

Kemp, W.M., W.R. Boynton, J.E. Adolf, D.F. Boesch, W.C. Boicourt, G. Brush, J.C. Cornwell, T.R. Fisher, P.M. Glibert, J.D. Hagy, L.W. Harding, E.D. Houde, D.G. Kimmel, W.D. Miller, R.I.E. Newell,

M.R. Roman, E.M. Smith, and J.C. Stevenson. 2005. Eutrophication of Chesapeake Bay: Historical trends and ecological interactions. *Marine Ecology Progress Series* 303: 1–29.

Kemp, A.C., B.P. Horton, S.J. Culver, D.R. Corbett, O. van de Plassche, W.R. Gehrels, B.C. Douglas, and A.C. Parnell. 2009. Timing and magnitude of recent accelerated sea-level rise (North Carolina, United States). *Geology* 37 (11): 1035–1038. https://doi.org/10.1130/G30352A.1.

Lang, D.J. 1982. Water quality of the three major tributaries to the Chesapeake Bay, the Susquehanna, Potomac, and James Rivers, January 1979 - April 1981. *US Geological Survey Water-Resources Investigations*: 82–32.

Langland, M.J. 2009. *Bathymetry and sediment-storage capacity change in three reservoirs on the Lower Susquehanna River, 1996–2008*. 2009–5110. Scientific Investigations. US Geological Survey.

Langland, M.J. 2015. Sediment transport and capacity change in three reservoirs, lower Susquehanna River basin, Pennsylvania and Maryland 1900-2012. USGS Open-File Report 2014–1235.

Langland, M.J., and T.M. Cronin. 2003. *A summary report of sediment processes in Chesapeake Bay and watershed*. 03–4123. Water-Resoureces investigations. New Cumberland, PA.

Langland, M.J., and R.A. Hainly. 1997. *Changes in bottom-surface elevations in three reservoirs on the lower Susquehanna River, Pennsylvania and Maryland, following the January 1996 flood - implications for nutrient and sediment loads to Chesapeake Bay*. 97–4138. Water-Resources Investigations. US Geological Survey.

Lefcheck, J.S., R.J. Orth, W.C. Dennison, D.J. Wilcox, R.R. Murphy, J. Keisman, C. Gurbisz, M. Hannam, J.B. Landry, K.A. Moore, C.J. Patrick, J. Testa, D.E. Weller, and R.A. Batiuk. 2018. Long-term nutrient reductions lead to the unprecedented recovery of a temperate coastal region. *Proceedings of the National Academy of Sciences* 115 (14): 3658–3662. https://doi.org/10.1073/pnas.1715798115.

Lehtoranta, J., P. Ekholm, and H. Pitkänen. 2009. Coastal eutrophication thresholds: A matter of sediment microbial processes. *Ambio: A Journal of the Human Environment* 38 (6): 303–308. https://doi.org/10.1579/09-A-656.1.

Li, M., L. Zhong, and W.C. Boicourt. 2005. Simulations of Chesapeake Bay estuary: Sensitivity to turbulence mixing parameterizations and comparison with observations. *Journal of Geophysical Research* 110 (C12). https://doi.org/10.1029/2004JC002585.

Li, M., L. Zhong, W.C. Boicourt, S. Zhang, and D.-L. Zhang. 2006. Hurricane-induced storm surges, currents and destratification in a semi-enclosed bay. *Geophysical Research Letters* 33 (2). https://doi.org/10.1029/2005GL024992.

Linker, L.C., R.A. Batiuk, G.W. Shenk, and C.F. Cerco. 2013. Development of the Chesapeake Bay watershed Total maximum daily load allocation. *JAWRA Journal of the American Water Resources Association: n/a-n/a.* https://doi.org/10.1111/jawr.12105.

Liu, Y., B.A. Engel, D.C. Flanagan, M.W. Gitau, S.K. McMillan, and I. Chaubey. 2017. A review on effectiveness of best management practices in improving hydrology and water quality. *Science of the Total Environment* 601–602: 580–593. https://doi.org/10.1016/j.scitotenv.2017.05.212.

Malarkey, J., C.F. Jago, R. Hübner, and S.E. Jones. 2013. A simple method to determine the settling velocity distribution from settling velocity tubes. *Continental Shelf Research* 56: 82–89. https://doi.org/10.1016/j.csr.2013.01.018.

Malpezzi, M.A., L.P. Sanford, and B.C. Crump. 2013. Abundance and distribution of transparent exopolymer particles in the estuarine turbidity maximum of Chesapeake Bay. *Marine Ecology Progress Series* 486: 23–35. https://doi.org/10.3354/meps10362.

Mcnair, J.N., and J.D. Newbold. 2001. Turbulent transport of suspended particles and dispersing benthic organisms: The hitting-distance problem for the local exchange model. *Journal of Theoretical Biology* 209 (3): 351–369. https://doi.org/10.1006/jtbi.2001.2273.

Nichols, M.M. 1977. Response and recovery of an estuary following a river flood. *SEPM Journal of Sedimentary Research* 47. https://doi.org/10.1306/212F7301-2B24-11D7-8648000102C1865D.

Nixon, S.W. 2003. Replacing the Nile: Are anthropogenic nutrients providing the fertility once brought to the Mediterranean by a great river? *Ambio: A Journal of the Human Environment* 32 (1): 30–39. https://doi.org/10.1579/0044-7447-32.1.30.

North, E.W., S.Y. Chao, L.P. Sanford, and R.R. Hood. 2004. The influence of wind and river pulses on an estuarine turbidity maximum: Numerical studies and field observations in Chesapeake Bay. *Estuaries* 27 (1): 132–146. https://doi.org/10.1007/BF02803567.

NRC. 2011. *Achieving nutrient and sediment reduction goals in the Chesapeake Bay: An evaluation of program strategies and implementation*. Washington, D.C: National Academies Press. https://doi.org/10.17226/13131.

Officer, C.B., D.R. Lynch, G.H. Setlock, and G.R. Helz. 1984. Recent sedimentation rates in Chesapeake Bay. In *The estuary as a FIlter*, 131–157. Academic Press, Inc.

Olabarrieta, M., J.C. Warner, and N. Kumar. 2011. Wave-current interaction in Willapa Bay. *Journal of Geophysical Research* 116 (C12). https://doi.org/10.1029/2011JC007387.

Olsen, C.R., I.L. Larsen, P.D. Lowry, N.H. Cutshall, and M.M. Nichols. 1986. Geochemistry and deposition of ^{7}Be in river-estuarine and coastal waters. *Journal of Geophysical Research* 91 (C1): 896–908. https://doi.org/10.1029/JC091iC01p00896.

Orth, R.J., and K.A. Moore. 1984. Distribution and abundance of submerged aquatic vegetation in Chesapeake Bay: An historical perspective. *Estuaries* 7 (4): 531–540.

Orth, R.J., W.C. Dennison, J.S. Lefcheck, C. Gurbisz, M. Hannam, J. Keisman, J.B. Landry, K.A. Moore, R.R. Murphy, C.J. Patrick, J. Testa, D.E. Weller, and D.J. Wilcox. 2017. Submersed aquatic vegetation in Chesapeake Bay: Sentinel species in a changing world. *BioScience* 67 (8): 698–712. https://doi.org/10.1093/biosci/bix058.

Owen, M.W. 1976. *Determination of the settling velocities of cohesive muds. IT161*. Wallingford: Hydraulics Research Station.

Owens, M.S., and J.C. Cornwell. 2016. The benthic exchange of O_2, N_2, and dissolved nutrients using small core incubations. *Journal of Visualized Experiments* 114: e54098.

Paerl, H.W. 2006. Assessing and managing nutrient-enhanced eutrophication in estuarine and coastal waters: Interactive effects of human and climatic perturbations. *Ecological Engineering* 26 (1): 40–54. https://doi.org/10.1016/j.ecoleng.2005.09.006.

Palinkas, C.M. 2009. The timing of floods and storms as a controlling mechanism for shelf deposit morphology. *Journal of Coastal Research* 255: 1122–1129. https://doi.org/10.2112/08-1041.1.

Palinkas, C.M., and C.A. Nittrouer. 2006. Clinoform sedimentation along the Apennine shelf, Adriatic Sea. *Marine Geology* 234 (1-4): 245–260. https://doi.org/10.1016/j.margeo.2006.09.006.

Palinkas, C.M. and E. Russ, 2019. Spatial and temporal patterns of sedimentation in an infilling reservoir. Catena 180: 120–131.

Palinkas, C.M., C.A. Nittrouer, R.A. Wheatcroft, and L. Langone. 2005. The use of ^{7}Be to identify event and seasonal sedimentation near the Po River delta, Adriatic Sea. *Marine Geology* 222–223: 95–112. https://doi.org/10.1016/j.margeo.2005.06.011.

Palinkas, C.M., J.P. Halka, M. Li, L.P. Sanford, and P. Cheng. 2014. Sediment deposition from tropical storms in the upper Chesapeake Bay: Field observations and model simulations. *Continental Shelf Research* 86: 6–16. https://doi.org/10.1016/j.csr.2013.09.012.

Palmieri, A., F. Shah, and A. Dinar. 2001. Economics of reservoir sedimentation and sustainable management of dams. *Journal of Environmental Management* 61 (2): 149–163. https://doi.org/10.1006/jema.2000.0392.

Park, K., H.V. Wang, S.-C. Kim, and J.-H. Oh. 2008. A model study of the estuarine turbidity maximum along the main channel of the upper Chesapeake Bay. *Estuaries and Coasts* 31 (1): 115–133. https://doi.org/10.1007/s12237-007-9013-8.

Parsons, T.R., Y. Maita, and C.M. Lalli. 1984. *A manual of chemical and biological methods for seawater analysis*. New York: Pergamon Press.

Pirmez, C., L.F. Pratson, and M.S. Steckler. 1998. Clinoform development by advection-diffusion of suspended sediment: Modeling and comparison to natural systems. *Journal of Geophysical Research - Solid Earth* 103 (B10): 24141–24157. https://doi.org/10.1029/98JB01516.

Poppe, L.J., S.J. Williams, and V.F. Paskevich. 2005. *USGS east-coast sediment analysis: procedures, database, and GIS data*. USGS open-file report 2005–1001.

Reed, L.A., and S.A. Hoffman. 1997. *Sediment deposition in Lake Clarke, Lake Aldred, and Conowingo Reservoir, Pennsylvania and Maryland, 1910–93*. USGS 96–4048. Water-Resources Investigations. Lemoyne, PA: USGS.

Roden, E.E., and J.W. Edmonds. 1997. Phosphate mobilization in iron-rich anaerobic sediments: Microbial Fe(III) oxide reduction versus iron-sulfide formation. *Archiv Fur Hydrobiologie* 139: 347–378.

Russ, E.R. 2019. Sediment connectivity between the lower Susquehanna River and upper Chesapeake Bay. PhD Dissertation, University of Maryland College Park.

Russ, E.R., and C.M. Palinkas. 2018. Seasonal-scale and decadal-scale sediment-vegetation interactions on the subaqueous Susquehanna River delta, upper Chesapeake Bay. *Estuaries and Coasts* 41 (7): 2092–2104. https://doi.org/10.1007/s12237-018-0413-8.

Russ, E.R., and C.M. Palinkas. In review. Sediment dynamics in upper Chesapeake Bay. *Estuarine, Coastal and Shelf Science*.

Sanford, L.P. 1994. Wave-forced resuspension of upper Chesapeake Bay muds. *Estuaries* 17 (1): 148. https://doi.org/10.2307/1352564.

Sanford, L.P., S.E. Suttles, and J.P. Halka. 2001. Reconsidering the physics of the Chesapeake Bay estuarine turbidity maximum. *Estuaries* 24 (5): 655–669.

Sanford, L.P., P.J. Dickhudt, L. Rubiano-Gomez, M. Yates, S.E. Suttles, C.T. Friedrichs, D.D. Fugate, and H. Romine. 2005. Variability of suspended particle concentrations, sizes, and settling velocities in the Chesapeake Bay turbidity maximum. *Flocculation in natural and engineered environmental systems*: 211–236.

Schnoor, J.L. 1996. *Environmental modeling: Fate and transport of pollutants in water, air, and soil*. John Wiley and Sons.

Schubel, J.R. 1968. Turbidity maximum of the northern Chesapeake Bay. *Science* 161 (3845): 1013–1015. https://doi.org/10.1126/science.161.3845.1013.

Schubel, J.R. 1972. Suspended sediment discharge of the susquehanna river at Conowingo, Maryland, during 1969. *Chesapeake Science* 13 (1): 53. https://doi.org/10.2307/1350551.

Schubel, J.R., and H.H. Carter. 1977. Suspended sediment budget for Chesapeake Bay. In *Estuarine Processes*, 48–62. Elsevier. doi: https://doi.org/10.1016/B978-0-12-751802-2.50012-6.

Schubel, J.R., and T.W. Kana. 1972. Agglomeration of fine-grained suspended sediment in northern Chesapeake Bay. *Powder Technology* 6 (1): 9–16. https://doi.org/10.1016/0032-5910(72)80050-0.

Sclavo, M., A. Benetazzo, S. Carniel, A. Bergamasco, F.M. Falcieri, and D. Bonaldo. 2013. Wave-current interaction effect on sediment dispersal in a shallow semi-enclosed basin. *Journal of Coastal Research* 165: 1587–1592. https://doi.org/10.2112/SI65-268.1.

Shchepetkin, A.F., and J.C. McWilliams. 2005. The regional oceanic modeling system (ROMS): A split-explicit, free-surface, topography-following-coordinate oceanic model. *Ocean Modelling* 9 (4): 347–404. https://doi.org/10.1016/j.ocemod.2004.08.002.

Shchepetkin, A.F., and J.C. McWilliams. 2009. Computational kernel algorithms for fine-scale, multiprocess, longtime oceanic simulations. In Handbook of Numerical Analysis, 14:121–183. Elsevier. doi:https://doi.org/10.1016/S1570-8659(08)01202-0.

Soulsby, R. 1997. *Dynamics of Marine Sands: A Manual for Practical Applications. Heron quay*. London: Thomas Telford Publications.

Syvitski, J.P., and M.D. Morehead. 1999. Estimating river-sediment discharge to the ocean: Application to the eel margin, northern California. *Marine Geology* 154 (1-4): 13–28.

Testa, J.M., and W.M. Kemp. 2012. Hypoxia-induced shifts in nitrogen and phosphorus cycling in Chesapeake Bay. *Limnology and Oceanography* 57 (3): 835–850. https://doi.org/10.4319/lo.2012.57.3.0835.

Testa, J.M., and W.M. Kemp. 2014. Spatial and temporal patterns of winter–spring oxygen depletion in Chesapeake Bay bottom water. *Estuaries and Coasts* 37 (6): 1432–1448. https://doi.org/10.1007/s12237-014-9775-8.

Testa, J.M., and W.M. Kemp. 2017. Modeling sediment nutrient and oxygen cycling in the Conowingo reservoir and upper Chesapeake Bay. [UMCES}CBL 2017-060. University of Maryland Center for Environmental Science.

Testa, J.M., D.C. Brady, D.M. Di Toro, W.R. Boynton, J.C. Cornwell, and W.M. Kemp. 2013. Sediment flux modeling: Simulating nitrogen, phosphorus, and silica cycles. *Estuarine, Coastal and Shelf Science* 131: 245–263. https://doi.org/10.1016/j.ecss.2013.06.014.

Testa, J.M., Y. Li, Y.J. Lee, M. Li, D.C. Brady, D.M. Di Toro, W.M. Kemp, and J.J. Fitzpatrick. 2014. Quantifying the effects of nutrient loading on dissolved O2 cycling and hypoxia in Chesapeake Bay using a coupled hydrodynamic–biogeochemical model. *Journal of Marine Systems* 139: 139–158. https://doi.org/10.1016/j.jmarsys.2014.05.018.

Testa, J.M., W.M. Kemp, and W.R. Boynton. 2018. Season-specific trends and linkages of nitrogen and oxygen cycles in Chesapeake Bay: Linked oxygen and nitrogen trends. *Limnology and Oceanography* 63 (5): 2045–2064. https://doi.org/10.1002/lno.10823.

Turner, R.E., and N.N. Rabalais. 1991. Changes in Mississippi River water quality this century. *BioScience* 41 (3): 140–147. https://doi.org/10.2307/1311453.

USGS. 2013. Surface-Water Data for the Nation.

Velleux, M., and J. Hallden. 2017. *Hydrodynamic and sediment transport analyses for Conowingo pond*. Mahwah: HDR.

Vericat, D., and R.J. Batalla. 2006. Sediment transport in a large impounded river: The lower Ebro, NE Iberian Peninsula. *Geomorphology* 79 (1-2): 72–92. https://doi.org/10.1016/j.geomorph.2005.09.017.

Vulgaropulos, Z. 2017. *Reservoir scour as a major source of bioavailable phosphorus to a coastal plain estuary? MS Thesis, College Park*. College Park: University of Maryland.

Warner, J.C., C.R. Sherwood, R.P. Signell, C.K. Harris, and H.G. Arango. 2008. Development of a three-dimensional, regional, coupled wave, current, and sediment-transport model. *Computers & Geosciences* 34 (10): 1284–1306. https://doi.org/10.1016/j.cageo.2008.02.012.

Warner, J.C., B. Armstrong, R. He, and J.B. Zambon. 2010. Development of a coupled ocean–atmosphere–wave–sediment transport (COAWST) modeling system. *Ocean Modelling* 35 (3): 230–244. https://doi.org/10.1016/j.ocemod.2010.07.010.

Warrick, J.A. 2015. Trend analyses with river sediment rating curves. *Hydrological Processes* 29 (6): 936–949. https://doi.org/10.1002/hyp.10198.

Xie, X., M. Li, and W. Ni. 2018. Roles of wind-driven currents and surface waves in sediment resuspension and transport during a tropical storm. *Journal of Geophysical Research, Oceans* 123 (11): 8638–8654. https://doi.org/10.1029/2018JC014104.

Yang, Z., H. Wang, Y. Saito, J.D. Milliman, K. Xu, S. Qiao, and G. Shi. 2006. Dam impacts on the Changjiang (Yangtze) river sediment discharge to the sea: The past 55 years and after the three gorges dam. *Water Resources Research* 42 (4). https://doi.org/10.1029/2005WR003970.

Zabawa, C.F., and J.R. Schubel. 1974. Geologic effects of tropical storm Agnes on upper Chesapeake Bay. *Maritime Sediments* 10: 79–84.

Zhang, Q., and W.P. Ball. 2014. *Data associated with long-term trends of nutrients and sediment from the nontidal Chesapeake watershed: An assessment of Progress by river and season*. Johns Hopkins University Data Archive Dataverse. https://doi.org/10.7281/T1VD6WC7.

Zhang, Q., and J.D. Blomquist. 2018. Watershed export of fine sediment, organic carbon, and chlorophyll-a to Chesapeake Bay: Spatial and temporal patterns in 1984–2016. *Science of the Total Environment* 619–620: 1066–1078. https://doi.org/10.1016/j.scitotenv.2017.10.279.

Zhang, Q., D.C. Brady, and W.P. Ball. 2013. Long-term seasonal trends of nitrogen, phosphorus, and suspended sediment load from the non-tidal Susquehanna River basin to Chesapeake Bay. *Science of the Total Environment* 452–453: 208–221. https://doi.org/10.1016/j.scitotenv.2013.02.012.

Zhang, Q., D.C. Brady, W.R. Boynton, and W.P. Ball. 2015. Long-term trends of nutrients and sediment from the nontidal Chesapeake watershed: An assessment of progress by river and season. *JAWRA Journal of the American Water Resources Association* 51 (6): 1534–1555. https://doi.org/10.1111/1752-1688.12327.

Zhang, Q., R.M. Hirsch, and W.P. Ball. 2016. Long-term changes in sediment and nutrient delivery from Conowingo dam to Chesapeake Bay: Effects of reservoir sedimentation. *Environmental Science & Technology* 50 (4): 1877–1886. https://doi.org/10.1021/acs.est.5b04073.

Zhang, Q., R.R. Murphy, R. Tian, M.K. Forsyth, E.M. Trentacoste, J. Keisman, and P.J. Tango. 2018. Chesapeake Bay's water quality condition has been recovering: Insights from a multimetric indicator assessment of thirty years of tidal monitoring data. *Science of the Total Environment* 637–638: 1617–1625. https://doi.org/10.1016/j.scitotenv.2018.05.025.

Zhong, L., and M. Li. 2006. Tidal energy fluxes and dissipation in the Chesapeake Bay. *Continental Shelf Research* 26 (6): 752–770. https://doi.org/10.1016/j.csr.2006.02.006.